ERDC/CERL TR-08-4

Construction Engineering
Research Laboratory

US Army Corps
of Engineers®
Engineer Research and
Development Center

Source Term Model for Fine Particle Resuspension from Indoor Surfaces

Yoojeong Kim, Ashok Gidwani, Mark Sippola, and Chang W. Sohn

February 2008

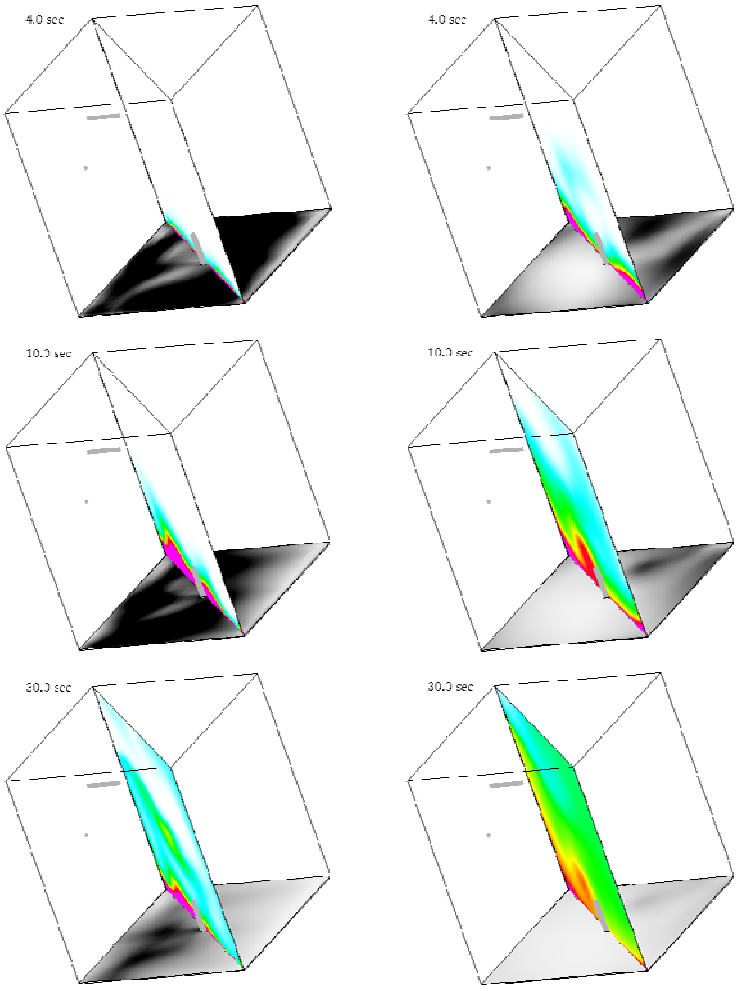

ERDC/CERL TR-08-4
February 2008

Source Term Model for Fine Particle Resuspension from Indoor Surfaces

Yoojeong Kim
Triton Systems, Inc.
200 Turnpike Road
Chelmsford, MA 01824

Ashok Gidwani
CFD Research Corporation
215 Wynn Drive
Huntsville, AL 35805

Mark Sippola
Lawrence Berkeley National Laboratory
1 Cyclotron Road
Berkeley, CA 94720

Chang W. Sohn
U.S. Army Engineer Research and Development Center
Construction Engineering Research Laboratory (CERL)
2902 Newmark Dr.
Champaign, IL 61824

Final Report

Prepared for U.S. Army Corps of Engineers
Washington, DC 20314-1000

Under Work Units F726C1 and J5LG71

Abstract: This Phase I effort developed a source term model for particle resuspension from indoor surfaces to be used as a source term boundary condition for CFD simulation of particle transport and dispersion in a building. Specifically, this work: (1) investigated responsible mechanisms for fine particle resuspension from indoor surfaces, (2) identified parameters relevant to resuspension, (3) performed a dimensional analysis and derivation of a resuspension model, and (4) evaluated the model against published experimental data on resuspension. Preliminary validation of the derived model was conducted based on a set of experimental data from the Lawrence Berkeley National Laboratory.

Contents

Figures and Tables

Figures

Tables

Preface

This study was conducted for the Engineer Research and Development Center, Construction Engineering Research Laboratory (ERDC-CERL) under MIPR No. 50633728 (FY05), "Experimental Determination of Particle Resuspension from Room Surfaces Due to Air Turbulence" and under Phase I SBIR Contract No. W9132T-07-C-0013, "Source Term Model for Fine Particle Resuspension from Indoor Surfaces," Work Unit F726C1, "Source Term Model for Fine Particles." The technical Monitor was Martin J. Savoie, CEERD-TD.

The work was performed by the Energy Branch (CF-E) of the Facilities Division (CF), Construction Engineering Research Laboratory (CERL). The CERL Principal Investigator was Dr. Chang W. Sohn. This work was partly done by the Lawrence Berkeley National Laboratory, Berkeley, CA and Triton Systems, Inc., Chelmsford, MA. Dr. Thomas A. Hartranft is Chief, CEERD-CF-E, and L. Michael Golish is Chief, CEERD-CF. The associated Technical Director was Mr. Martin J. Savoie, CEERD-TD. The Director of CERL is Dr. Ilker R. Adiguzel.

CERL is an element of the U.S. Army Engineer Research and Development Center (ERDC), U.S. Army Corps of Engineers. The Commander and Executive Director of ERDC is COL Richard B. Jenkins, and the Director of ERDC is Dr. James R. Houston.

Unit Conversion Factors

Multiply	By	To Obtain
cubic feet	0.02831685	cubic meters
cubic inches	1.6387064 E-05	cubic meters
cubic yards	0.7645549	cubic meters
degrees (angle)	0.01745329	radians
degrees Fahrenheit	(F-32)/1.8	degrees Celsius
feet	0.3048	meters
gallons (U.S. liquid)	3.785412 E-03	cubic meters
inches	0.0254	meters
inch-pounds (force)	0.1129848	newton meters
miles (nautical)	1,852	meters
miles (U.S. statute)	1,609.347	meters
miles per hour	0.44704	meters per second
mils	0.0254	millimeters
ounces (mass)	0.02834952	kilograms
ounces (U.S. fluid)	2.957353 E-05	cubic meters
pints (U.S. liquid)	4.73176 E-04	cubic meters
pints (U.S. liquid)	0.473176	liters
pounds (force)	4.448222	newtons
pounds (force) per foot	14.59390	newtons per meter
pounds (force) per inch	175.1268	newtons per meter
pounds (force) per square foot	47.88026	pascals
pounds (force) per square inch	6.894757	kilopascals
pounds (mass)	0.45359237	kilograms
quarts (U.S. liquid)	9.463529 E-04	cubic meters
square feet	0.09290304	square meters
square inches	6.4516 E-04	square meters
square miles	2.589998 E+06	square meters
square yards	0.8361274	square meters
tons (2,000 pounds, mass)	907.1847	kilograms
yards	0.9144	meters

1 Introduction

1.1 Background

How contaminants are dispersed inside buildings has long been a topic of interest to those seeking to improve indoor air quality (IAQ) in modern buildings. This topic also interests those seeking to protect against the potential for indoor dispersal of toxic contaminants, i.e., chemical and biological (CB) agents.

To design an active protection system or to develop successful countermeasure strategies against CB agents dispersed indoors requires detailed information on a room's dispersion profile. A number of computational fluid dynamics (CFD) codes capable of simulating contaminant dispersion inside a building already exist in the public and commercial domains (Gadgil et al. 2000; Sohn et al. 2004). However, to apply these CFD codes to calculate a dispersion profile first requires a prescription of boundary conditions; one of the critical boundary conditions affecting the simulation of contaminant dispersion profile is the "source term modeling."

In fiscal year 2007 (FY07), the Army Small Business Innovative Research (SBIR) program office funded a study of source term modeling for fine particle resuspension from indoor surfaces.* This Phase I study:

1. Investigated responsible mechanisms for fine particle resuspension from indoor surfaces
2. Identified parameters relevant to resuspension
3. Performed dimensional analysis and derivation of a resuspension model
4. Evaluated the model against published experimental data on resuspension.

This work, based on the results of the SBIR Phase I contract research performed from April through October 2007, was undertaken to develop a source term model for particle resuspension under indoor environment.

* Chemical and Biological Defense SBIR Program 2007.1 Solicitation, Topic Number: CBD07-109, *Source Term Model for Fine Particles off Indoor Surfaces*, accessible through URL: https://www.armysbir.com/portal/cbd071/menu.asp

1.2 Objective

The overall objective of this Phase I effort was to develop a source term model for particle resuspension under indoor environment to be used as a source term boundary condition for CFD simulation of particle transport and dispersion in a building. The specific objectives were to:

1. Determine the responsible mechanisms for fine particle resuspension from indoor surfaces
2. Identify governing parameters relevant to resuspension off indoor surfaces
3. Develop models for resuspension of fine particles
4. Evaluate the models against experimental data in the public domain.

1.3 Approaches

This work began with an exhaustive literature study of published work on the related subject. Figure 1 shows the six project tasks and the time in which they were accomplished.

1.4 Scope

This report describes work conducted for the Phase I activities described in Figure 1. The validation of the model against the controlled experiments in a prototype test chamber is beyond the scope of the Phase I work. The validation of the derived model through a series of experiments in a prototype test chamber is included in the Phase II SBIR proposal.

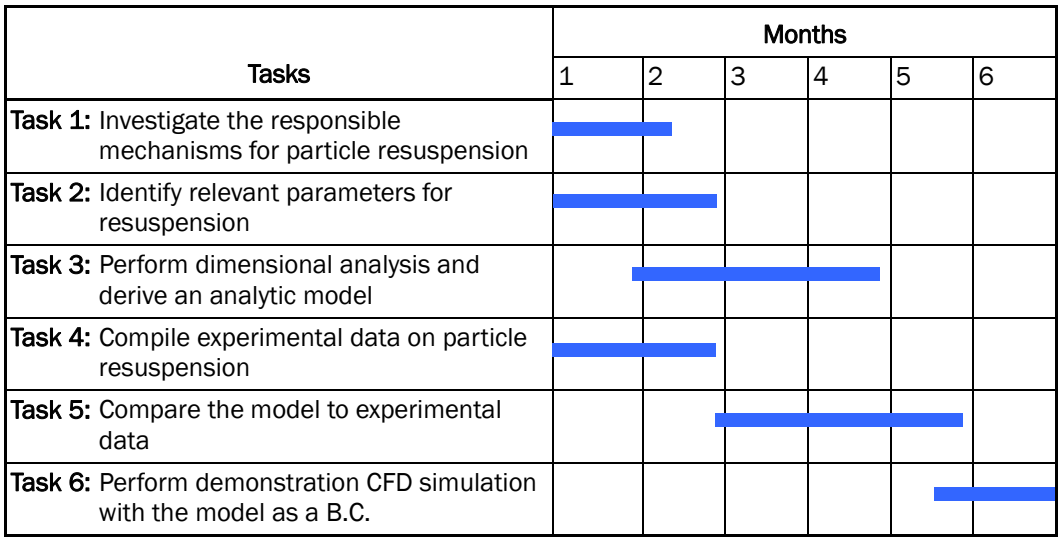

Figure 1. Gantt chart detailing Phase I study tasks.

1.5 Mode of Technology Transfer

It is anticipated that the results of this work will be submitted to a peer-reviewed journal. This report will be made accessible through the World Wide Web (WWW) at URL: http://www.cecer.army.mil.

2 Resuspension of Particles

Resuspension is the process by which particulate matter is introduced back into the air space from deposition surfaces; it is the net result of adhesion forces and removal forces acting on particles simultaneously over time. Resuspension plays a significant role in many environmental and industrial processes including: transport of radionuclides, exhaust emission and transport, spreading of crop diseases by fungal spores, cleaning of electronic chips, handling of toxic powders, transmission of human diseases, and distribution of allergens in indoor spaces (Gomes et al. 2005; Biasi et al. 2001).

Early scientific studies of resuspension processes were done in the field of erosion and soil transport. Development of nuclear technology led to research on resuspension of radionuclides as a cause of spreading airborne radioactivity from nuclear weapon test sites or from possible accidental release from the nuclear industry. Other studies in resuspension include the transport of hazardous particles from industrial spills and pesticides (Nicholson 1988). Recent interest in resuspension of particles in indoor environments has been raised as an important factor in indoor air quality (Thatcher and Layton 1995; Hu et al. 2005).

The anthrax attacks on U.S. Postal Service facilities and the Hart Senate Office Building in 2001 demonstrated that the release of a small amount of CB agents in a building is a very effective method of terrorism that poses a serious threat to the building occupants' safety and that can disable critical governmental functions. Airborne CB agents released in one section of a building travel via the building's heating, ventilating, and air-conditioning (HVAC) systems and disperse throughout the building, while undergoing deposition and resuspension recurrently.

To provide proper protection from CB agents, to design countermeasure devices, and to plan decontamination schemes, it is important to understand how CB agents migrate through a building. CFD has been employed to simulate dispersion of CB agents in a building through HVAC systems. How well the simulation result would match the actual dispersion profile of CB agents depends on the accuracies of models describing the physical phenomena such as aerodynamic characteristics of CB agents and fluid motions through HVAC systems. One of the important factors, not well es-

tablished, is the resuspension mechanism of fine particles. This is due to the complexity of the turbulent boundary layer where particles reside and the chemistry of particle and surface interactions (Loosmore 2003). Resuspension models currently used are simple and inadequate for describing short-term resuspension, which is important in indoor environments. Therefore, a resuspension model that characterizes indoor resuspension appropriately is needed that would improve the accuracy of simulation of CB agent dispersal in a building.

2.1 Resuspension Mechanism

Resuspension is a net result of adhesion forces and removal forces exerting concurrently on particles deposited on a surface. This section examines adhesion and removal forces.

2.1.1 Adhesion Forces

The main adhesion forces between a particle and a surface are the van der Waals force, the capillary force, and the electrostatic force.

2.1.1.1 The van der Waals Force

Equation 1 describes (and Figure 2 shows) the van der Waals force between a particle and a near surface without considering contact angle flattening:

$$F_{\mathrm{vdW}} = \frac{A_{132} d_{\mathrm{p}}}{12 s^2} \qquad \text{Eq 1}$$

where:

A_{132}= the Hamaker constant
d_{p} = the particle diameter
s = the separation distance between the particle and the surface.

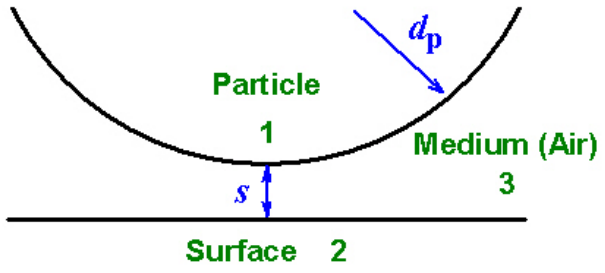

Figure 2. Van der Waals force between particle and plane.

The Hamaker constant, A_{132}, expresses dipole interactions between two materials (Particle 1 and Surface 2) in a medium (3, air) macroscopically:

$$A_{132} = A_{12} + A_{33} - A_{13} - A_{23} \quad \text{Eq 2}$$

where:

$$A_{ij} \cong \sqrt{A_{ii} A_{jj}} \quad \text{Eq 3}$$

Combining Equations 2 and 3 results in:

$$A_{132} \cong (\sqrt{A_{11}} - \sqrt{A_{33}})(\sqrt{A_{22}} - \sqrt{A_{33}}) \quad \text{Eq 4}$$

Real particles are not perfectly rigid, but deform under the influence of this adhesive force. If the adhesion surface area is increased from point contact to a circle of radius r_{adhesion}, then the van der Waals adhesion force increases to:

$$F_{\text{vdW}} = \frac{A_{132} d_{\text{p}}}{12 s^2} + \frac{2 A_{132} r_{\text{adhesion}}}{12 s^3} \quad \text{Eq 5}$$

Equation 6 describes (and Figure 3 shows) van der Waals force between two planar surfaces:

$$\frac{F_{\text{vdW}}}{Area} = \frac{A_{132}}{6 s^3} \quad \text{Eq 6}$$

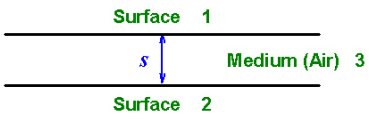

Figure 3. Van der Waals force between planes.

2.1.1.2 Capillary Force

Depending on the relative humidity (RH) level, water can condense in the gap between a particle and a surface resulting in an adhesion force caused by surface tension. The capillary force is given as:

$$F_{\text{C}} = 2\pi\gamma_{\text{LV}} d_{\text{p}} \quad \text{Eq 7}$$

where:

γ_{LV} = the liquid-gas surface tension.

2.1.1.3 Electrostatic Force

The electrostatic force due to electrostatic double layer is expressed as:

$$F_{\mathrm{EDL}} = \pi \varepsilon_0 \frac{d_{\mathrm{p}}}{2} \frac{\phi_{\mathrm{c}}^{\ 2}}{s} \qquad \text{Eq 8}$$

where:

ϕ_{c} = the contact potential
ε_0 = the dielectric constant.

In case of charged particles, the electrostatic force due to a charged particle is:

$$F_{\mathrm{Q}} = \frac{1}{4\pi\varepsilon_0} \frac{q^2}{(d_{\mathrm{p}} + 2s)^2} \qquad \text{Eq 9}$$

where:

q = the charge on the particle.

2.1.1.4 Empirical Correlation

Hinds (1999) derived an empirical equation for adhesion force for hard particles and clean surfaces:

$$F_{\mathrm{adh}} = 15 d_{\mathrm{p}} (0.5 + 0.0045 (\%\mathrm{RH})) \qquad \text{Eq 10}$$

The units for F_{adh} and d_{p} are N and μm, respectively. The RH term in Equation 10 reflects the importance of the capillary force in adhesion forces.

2.1.2 Removal Forces

A removal force is required to dislodge particles from a surface. A removal force can be mechanical, centrifugal, vibrational, or hydrodynamic. This section considers only the hydrodynamic force. Particles on a surface are subjected to shear stress in the viscous sub-layer of the turbulent boundary layer, which results in the lift and the drag forces.

2.1.2.1 Lift Force

The shear lift originates from inertia effects in the viscous flow around the particle. The expression for the inertia shear lift, first obtained by Saffman (1965; 1968) can be restated for a particle resting on a surface as:

$$\frac{F_L}{\rho_a \nu^2} = 0.807\left(\frac{d_p u_*}{\nu}\right)^3 \quad \text{Eq 11}$$

where:

ρ_a = the density of air
ν = the kinematic viscosity of air
u_* = the friction velocity.

Alternatively, Leighton and Acrivos (1985) found:

$$\frac{F_L}{\rho_a \nu^2} = 0.576\left(\frac{d_p u_*}{\nu}\right)^4 \quad \text{Eq 12}$$

Hall (1988) derived an empirical correlation for the mean lift force as:

$$\frac{\langle F_L \rangle}{\rho_a \nu^2} \approx 20.9\left(\frac{d_p u_*}{2\nu}\right)^{2.31} \text{ for } 1.8 < \frac{d_p u_*}{2\nu} < 70 \quad \text{Eq 13}$$

2.1.2.2 Drag Force

The drag force for a particle on a surface is given by Punjrath and Heldman (1972):

$$F_D = \frac{C_{fx}\rho_a U_\infty^2}{2}\left(\frac{\pi d_p^2}{4}\right) \quad \text{Eq 14}$$

where:

C_{fx} = the local shear stress coefficient
U_∞ = the free stream air flow velocity.

Hall (1988) derived an empirical correlation for the mean drag force:

$$\frac{\langle F_D \rangle}{\rho_a \nu^2} \approx 32\left(\frac{d_p u_*}{2\nu}\right)^2 \quad \text{Eq 15}$$

2.2 Existing Models of Resuspension

2.2.1 Resuspension Factor *K* and Resuspension Rate Λ

The most frequently used terms for describing resuspension are the resuspension factor K and the resuspension rate Λ. The resuspension factor is defined as:

$$K\,[\mathrm{m}^{-1}] = \frac{\text{airborne concentration}\,[\mathrm{g\ m}^{-3}]}{\text{initial surface concentration}\,[\mathrm{g\ m}^{-2}]} \qquad \text{Eq 16}$$

The airborne concentration is measured at some reference height, which is usually the breathing height. The resuspension rate Λ is defined as the fraction removed in unit time, more explicitly:

$$\Lambda\,[\mathrm{s}^{-1}] = \frac{\text{resuspension flux}\,[\mathrm{g\ m}^{-2}\mathrm{s}^{-1}]}{\text{initial surface concentration}\,[\mathrm{g\ m}^{-2}]} \qquad \text{Eq 17}$$

The relationship between K to Λ is given, assuming the particle concentration follows a power law distribution with height by (Loosmore 2003):

$$\Lambda = u_* \kappa p K \qquad \text{Eq 18}$$

with:

$$p = \frac{V_\mathrm{d}\varphi}{u_*\kappa} \qquad \text{Eq 19}$$

where:

κ = the von Karman constant
V_d = the turbulent deposition velocity

The diabatic influence function φ has a value of 1 for neutral conditions, <1 for unstable conditions, and >1 for stable conditions.

The value for p has been calculated to be in the range of 0.05 to 0.5 with a median value of 0.18.

2.2.2 Empirical Models

Table 1 lists empirical models for the resuspension factor K, which decreases exponentially or inversely with time.

Table 1. Models for the resuspension factor *K*.

Model*	
$K = 10^{-5}\exp(-0.0139t) + 10^{-9}$ (Source: USAEC 1972)	Eq 20
$K = 10^{-5}\exp(-0.00185t) + 10^{-9}$ (Source: USAEC 1975)	Eq 21
$K = 10^{-4}\exp(-0.15\sqrt{t}) + 10^{-9}$ (Anspaugh et al. 1975)	Eq 22
$K = 10^{-6}\exp(-0.01t) + 10^{-9}$ (Linsley 1978)	Eq 23
$K = \frac{1.2\times10^{-6}}{t}$ (Garland 1979)	Eq 24
$K = 10^{-6}$ for $t < 1$ day ; $K = \frac{10^{-6}}{t}$ for $1 < t < 1000$ days (NCRP 1999)	Eq 25
$K = [10^{-5}\exp(-0.07t) + 6\times10^{-9}\exp(-0.003t) + 10^{-9}]\times10^{\pm1}$ (Anspaugh et al. 2002)	Eq 26
$K = \frac{10^{-6}}{t}$ for $t < 1000$ days (Loosmore's (2003) adaptation of NCRP 1999)	Eq 27
* The units for *K* are m^{-1} and *t* is in days.	

Loosmore tested the applicability of the existing models (Equations 22, 25, 26, and 27 in Table 1) to short-term resuspension occurring within the first 24 hrs and found that only Equation 27 is adequate to describe short-term resuspension (Loosmore 2003). The author also developed two empirical models, one extensive and the other simplified, for short-term resuspension using published data. The extensive model (Loosmore 2003) is expressed as:

$$\Lambda = 0.42\frac{u_*^{2.13} d_p^{0.17}}{t^{0.92} z_0^{0.32} \rho_p^{0.76}} \qquad \text{Eq 28}$$

where:

ρ_p = the particle density

z_o = the aerodynamic surface roughness length.

The simplified model developed by Loosmore is shown as:

$$\Lambda = 0.01\frac{u_*^{1.43}}{t^{1.03}} \quad \text{Eq 29}$$

where (for Equations 28 and 29):

Λ is in s^{-1}
u_* is in m/s
t is in s
d_p is in μm
ρ_p is in kg/m^3
z_o is in m.

Lengweiler et al. concluded that the air velocity, turbulence level, and surface orientation play a major role in deposition and resuspension (Lengweiler et al. 1998). Lengweiler derived empirical correlations address that the resuspension rate Λ [s^{-1}] is proportional to turbulent kinetic energy k [m^2/s^2] for floor, wall, and ceiling separately (Lengweiler 2000). They are:

$$\Lambda = 1.85\times10^{-4}k \quad \text{(for floor)} \quad \text{Eq 30}$$

$$\Lambda = 2.37\times10^{-4}k + 1.08\times10^{-4} \quad \text{(for wall)} \quad \text{Eq 31}$$

$$\Lambda = 3.94\times10^{-4}k + 1.47\times10^{-4} \quad \text{(for ceiling)} \quad \text{Eq 32}$$

2.2.3 Theoretical Models

Wen and Kasper (1989) developed a kinetic 'particle desorption' model in analogy to the desorption of molecules from heterogeneous surfaces. Particles on the surface have a distribution of adhesion forces; the total particle density on the surface is obtained by integrating the particle density (as a function of adhesion force) over the entire range of the adhesion force:

$$N_T = \int_0^\infty N(F)dF \quad \text{Eq 33}$$

The change in the number density of particles with the adhesion force F on the surface with time is given as:

$$\frac{dN(F)}{dt} = -aN(F) \quad \text{Eq 34}$$

where:

$N(F)$ = the number density of particles with the adhesion force F on the surface.
a = the rate constant.

The first order rate constant is a function of the non-dimensional adhesion force, *F*, and analogous to the Arrhenius formula:

$$a(F) = Ae^{-F} \quad \text{Eq 35}$$

with:

$$F = \frac{\text{adhesion force}}{\text{removal force}} \quad \text{Eq 36}$$

For *F*, Wen and Kasper (1989) used a uniform initial distribution. Jurcik and Wang (1991) developed instead a kinetic model with the concept of distributions of adhesion and removal forces. They assumed that adhesion forces have a log-normal distribution and removal forces have a Gaussian distribution.

The above-mentioned kinetic models are also called force balance models. These models are assuming that there is a threshold for removal based on a balance between the instantaneous aerodynamic removal force and particle surface adhesive forces. Once the threshold is exceeded, the rate of removal is determined by the frequency of the turbulent bursts.

Braaten developed a force balance model based on a Monte-Carlo approach instead of a kinetic approach (Braaten 1994). His model assumes that aerodynamic forces are applied to the particle on the surface in discrete bursts. The values of these forces are derived from some prescribed probability distribution; resuspension occurs when the force exceeded the local adhesive force, which was given a log-normal distribution. This kind of model is heavy on computing time, but offers a direct way of implementing the physical process via the particle equation of motion (Biasi et al. 2001).

Reeks et al. (1988) described resuspension as a process whereby particles reside in potential wells formed by attractive and repulsive forces. The particles are also subject to lift forces with mean and fluctuating components generated by turbulent flow over the surface. Resuspension occurs when the particle acquires enough energy to escape from the potential well; therefore, this model is also called a dynamic energy accumulation model. Recently, Reeks and Hall (2001) developed the dynamic “rock and roll” model with resonant energy transfer. This model accounts for influence of drag through accumulation of rotational energy through the rocking of a particle about the surface asperities in the contact zone.

2.3 Responsible Parameters for Resuspension

Resuspension is governed by adhesion and removal forces. Parameters that affect these forces include: the size and the shape of particle, the material characteristics of particles, the roughness of the surface, the material characteristics of the surface, the friction velocity, the turbulent level of the flow, the relative humidity, the temperature, and the duration of contact (Hinds 1999).

As shown in Section 2.1 (p 5), there is an agreement between different models, whether theoretical or empirical, that in general, adhesion forces are proportional to d_p while removal forces are proportional to d_p^2 or d_p^3. This indicates that, as the size of particles decreases, adhesion forces become greater than removal forces. Corn and Stein (1965) showed experimentally that removal of particles increased with increasing particle size. The dependence of removal efficiency on particle size was partly explained by the smallest particles becoming enclosed in the viscid boundary later and not being easily removed (Nicholson 1988). Larger particles stick up higher into the boundary layer and are subject to higher removal forces (Loosmore 2003).

Corn and Stein (1965) reported that particle adhesion increased with increasing relative humidity, probably due to increasing capillary force. The relative humidity also has an effect on the electrostatic force. Higher relative humidity results in faster leakage of electrostatic charge thus changing the charge on particles.

The equations in Section 2.1 for adhesion and removal forces pertain to smooth surfaces; they do not take the surface roughness into account. Adhesion forces decrease with increasing surface roughness, which is due to increasing separation distance. However, experimental data showed that the removal of particles decreased with increasing surface roughness (Corn and Stein 1965). Loosemore (2003) explained that larger surface roughness provides more shielding, which acts against resuspension.

Time dependence of resuspension has been reported in many studies. The resuspension flux is shown to decrease nonlinearly with time after deposition. Nicholson's (1993) wind tunnel experiments showed that nearly 50 percent of the total resuspension occurred within the first 10 seconds in many trials. This is believed to be due to the fact that particles with the smallest adhesive forces are thought to be removed immediately after deposition, leaving behind a more firmly held contaminant reservoir

(Clever and Yates 1973; Ziskind et al. 1995; Zimon 1969). Linsley described that the resuspension factor decreases exponentially with time (Linsley 1978). Garland found that an inverse power law fit his wind tunnel data for times varying from several minutes to a number of months (Garland 1979). It is widely accepted that the resuspension factor is proportional to $1/t^n$ where n is some power slightly greater than 1.

3 Development of Indoor Resuspension Models of Fine Particles

3.1 Identification of Relevant Parameters

The following parameters were identified as important for the resuspension rate Λ [s^{-1}] based on the responsible mechanisms for particle resuspension:

d_p: particle diameter (m)
ρ_p: particle density (kg/m^3)
t: time (s)
u_*: friction velocity (m/s)
ε: turbulent intensity (turbulent energy dissipation rate) (m^2/s^3)
p_t: turbulent pressure ($kg/m/s^2$)
z_o: surface roughness length (m)
A_{132}: Hamaker constant ($kg \cdot m^2/s^2$)
RH: relative humidity
γ_{LV}: liquid-gas surface tension (kg/s^2)
ρ_a: air density (kg/m^3)
μ_a: air viscosity (kg/m/s)
g: gravity (m/s^2).

Particle properties are the diameter and the density; the surface roughness length characterizes the surface. Friction velocity, turbulent intensity, and relative humidity are environmental conditions. There should also be a parameter or parameters that differentiate types of particles (e.g., spores, TiO_2, silica, etc.) and types of surfaces (e.g., carpet, wood, concrete, vinyl etc.). The Hamaker constant is regarded here to be one.

This study also considered thermophoresis, which describes the motion of suspended particles induced by temperature gradients in fluid. Thermophoresis may play a role in dispersion of particles (and CB agents) in a building through HVAC systems, especially in summer or winter when air conditioning or heating, respectively, is used. It may also enhance or reduce particle deposition if the temperature difference between walls and the ambient is considerable. However, the effect of the difference between the ambient temperature and the wall's temperature on deposited particles and the magnitude of the resulting forces compared to van der Waals forces are unknown. Therefore, neither the temperature nor the temperature difference in the above was included.

3.2 Dimensional Analysis

3.2.1 Case 1

With all the variables listed above, the resuspension rate is expressed as a function of 13 variables:

$$\Lambda = f(d_p, \rho_p, t, u_*, \varepsilon, \mathrm{RH}, z_0, A_{132}, \rho_a, \mu_a, p_t, g, \gamma_{LV}) \quad \text{Eq 37}$$

In Equation 37, there are a total of 14 parameters and three repeating units: mass, length, and time. Using the Buckingham $\prod$ theorem, the minimum number of unique dimensionless parameters is 11; d_p, u_*, and ρ_a were chosen as the three repeating parameters that encompass all three dimensions, and the resulting equation becomes:

$$\frac{\Lambda d_p}{u_*} = f\left(\frac{\rho_p}{\rho_a}, \frac{u_* t}{d_p}, \frac{\varepsilon d_p}{u_*^3}, \mathrm{RH}, \frac{z_0}{d_p}, \frac{A_{132}}{d_p^3 u_*^2 \rho_a}, \frac{\mu_a}{d_p u_* \rho_a}, \frac{p_t}{u_*^2 \rho_a}, \frac{g d_p}{u_*^2}, \frac{\gamma_{LV}}{d_p u_*^2 \rho_a}\right) \quad \text{Eq 38}$$

3.2.2 Case 2

To derive empirical correlations from Equation 38 requires experimental data that contain information on all 10 independent variables. However, most resuspension experiments in literature do not specify values of ε and p_t. Therefore, it is not possible to include ε and p_t as variables for resuspension rate.

Some of variables in Equation 37 do not change or are relatively constant. The liquid-gas surface tension of interest is only the surface tension of water at the air interface for the particle resuspension. Therefore, the value of γ_{LV} does not vary among experiments, and can be excluded in Equation 37. Since the goal of this work is to develop an indoor resuspension model, the range of ambient temperature is relatively small. Furthermore, most of experiments were performed between 20 and 25 °C. Since the viscosity of air is primarily a function of temperature with a minor dependency on pressure, the variation of the air viscosity would be very small and can be omitted from Equation 37.

Reeks and Hall (2001) noted that, in practice, the contribution from gravity is much smaller than that from the drag force, although it may be important in re-establishing contact with the surface once the contacts have been broken (Ziskind 2006). Therefore, Equation 37 can disregard gravity.

After considering these aspects, Equation 37 can be rewritten as:

$$\Lambda = f(d_p, \rho_p, t, u_*, \text{RH}, z_0, A_{132}, \rho_a) \quad \text{Eq 39}$$

and the resulting dimensionless variables by choosing d_p, u_*, and ρ_a as the three repeating parameters are:

$$\frac{\Lambda d_p}{u_*} = f\left(\frac{\rho_p}{\rho_a}, \frac{u_* t}{d_p}, \text{RH}, \frac{z_0}{d_p}, \frac{A_{132}}{d_p^{\,3} u_*^{\,2} \rho_a}\right) \quad \text{Eq 40}$$

3.2.3 Case 3

The density of air is a function of pressure and temperature. In indoor environments, the ambient pressure and the temperature are relatively constant. Therefore, the above reasoning for considering the viscosity of air constant can be applied to the density of air, and the relevant parameters can be further reduced for the resuspension as:

$$\Lambda = f(d_p, \rho_p, t, u_*, \text{RH}, z_0, A_{132}) \quad \text{Eq 41}$$

with:

d_p, u_*, and ρ_p, instead of ρ_a, as the three repeating parameters, thus:

$$\frac{\Lambda d_p}{u_*} = f\left(\frac{u_* t}{d_p}, \text{RH}, \frac{z_0}{d_p}, \frac{A_{132}}{d_p^{\,3} u_*^{\,2} \rho_p}\right) \quad \text{Eq 42}$$

3.2.4 Case 4

To be thorough, this case was added to include the viscosity of air to Equation 39. As a result:

$$\Lambda = f(d_p, \rho_p, t, u_*, \text{RH}, z_0, A_{132}, \rho_a, \mu_a) \quad \text{Eq 43}$$

Using d_p, u_*, and ρ_a as the three repeating parameters again:

$$\frac{\Lambda d_p}{u_*} = f\left(\frac{\rho_p}{\rho_a}, \frac{u_* t}{d_p}, \text{RH}, \frac{z_0}{d_p}, \frac{A_{132}}{d_p^{\,3} u_*^{\,2} \rho_a}, \frac{\mu_a}{d_p u_* \rho_a}\right) \quad \text{Eq 44}$$

The last dimensionless variable in Equation 44 is 1/Re.

3.3 Model Development

Two different routes were pursued for model development: (1) to develop empirical correlations, and (2) to derive a model based on physics involved in resuspension using a moment balance between adhesion and removal.

3.3.1 Empirical Correlations

3.3.1.1 Experimental Data Used To Develop Empirical Correlations

Experimental data were collected from references by Ibrahim (2004), Nicholson (1993), Giess et al. (1997), Braaten et al. (1990), Wu et al. (1992), Krauter and Biermann (2007), and Wen and Kasper (1989). Among these data, Ibrahim's were the most extensive and encompassed effects of the relative humidity and different particle sizes, densities, and materials. However, only one surface material (glass) was used for studying resuspension. Therefore, another data set from a study using different surface materials was needed. Consequently, this work used the data by Ibrahim (2004) and Nicholson (1993) to obtain empirical correlations. The data were not used for deriving empirical correlations, but were used to test the performance of the empirical correlations.

Table 2 lists the parameters used for the experimental works by Ibrahim and Nicholson. One distinctive characteristic of Ibrahim's experiments was that the air flow was transient, meaning the velocity of the flow linearly accelerated from 0 m/s to a set value, whereas most of experiments in literature used a constant free steam velocity. In addition, Ibrahim also used larger (d_p = ~ 70 μm) and heavier particles (ρ_p = 8000 kg/m^3) than those used in most of literature.

Ibrahim measured the surface height distribution of glass using atomic force microscopy (AFM). The standard deviation of the height ranged from 1.08 nm to 13.75 nm with the mean of the standard deviation of 1.7 nm. Because the physical roughness or the effective obstacle height is usually estimated by the difference between the lowest and the highest points for a surface, the highest value, 13.75 nm, was taken as the standard deviation value for the glass surface. If one can assume the height has a normal distribution, 99.7 percent of the values are within three standard deviations. Therefore, the physical roughness was calculated as three times the standard deviation. The physical roughness of grass in Nicholson's data was given. Loosmore (2003) assumed the physical roughness for concrete in Nicholson's to be 3 mm, and this work used the same value. Loosmore estimated the aerodynamic roughness length as 1/10 of the physical roughness. Krauter and Biermann (2007) used 1/30 of the physical roughness as the aerodynamic roughness based on the work by Sutton (1955). Here, 1/10 of the physical roughness was used as the aerodynamic roughness length.

Table 2. Experimental parameters for works by Ibrahim (2004) and Nicholson (1993).

	Ibrahim (2004)	Nicholson (1993)
Dimensions for flow passage	Wind tunnel, 0.203 m × 0.203 m	Wind tunnel, 1 m × 1 m
Surface material	Glass	Grass and concrete
U_∞ (m/s)	Transient, 0 – 20	For grass: 3.0, 4.5, 8.0 For concrete: 3.0, 5.0, 6.5
u_* (m/s)	$u_* = 0.0375U_\infty + 0.0387$	For grass: 0.15, 0.3, 0.4 For concrete: 0.1, 0.15, 0.2
Particle	Stainless steel (SS) spheres, glass spheres, Lycopodium spores	Silica spheres
d_p (μm)	SS: 70, glass: 72, 32, Lycopodium: 30	4.1, 9.6, 17.5, 22.1 for most exp.'s 4.8, 8.6, 12.1, 16.5 for 1 set
ρ_p (kg/m^3)	SS: 8000, Glass: 2420, Lycopodium: 1000	1000
Surface feature height (m)	4.1×10^{-8}	Grass: 0.05, concrete: 0.003
Aerodynamic roughness (m)	4.1×10^{-9}	Grass: 0.005, concrete: 0.0003
Temperature (°C)	23	Not reported, assumed to be 25
RH (%)	Varied,18 – 67	Not reported
Resuspension rate	Computed from detachment fraction using Figs. 5.2, 5.3, 5.4, 5.7, 5.9, 6.2, 6.5, 8.1 in Ibrahim (2004)	Taken from Fig. 2 in Nicholson (1993)
Number of data points	443	96

Ibrahim's data (2004) were presented as the detachment fraction vs. the free stream velocity. The velocity linearly accelerated during the experiments as mentioned earlier, and therefore the velocity was converted to time using the acceleration value. Once graphs were obtained as the detachment fraction vs. time, then resuspension rate was calculated by taking a slope between two adjacent points. For the corresponding time for the obtained resuspension rate, two different approaches can be used as discussed by Nicholson (1993) and Loosmore (2003). The simplest approximation for the corresponding time is to use the mid-point of the period. An alternative approach is to assign the representative time to reflect the fact that the resuspension rate falls inversely proportionally to the time. The corresponding time t' for the calculated resuspension rate can be obtained by:

$$\frac{1}{t'} = \frac{1}{t_2 - t_1}\int_{t_1}^{t_2}\frac{1}{t}dt \qquad \text{Eq 45}$$

Here, it was decided to use both the mid-point and t' to draw empirical correlations and compare the results. Nicholson's data were taken directly from Figure 2 in Nicholson (1993), in which the mid-point time was used for the corresponding time for the measured resuspension rate. Since the sampling intervals were given in the reference, t' was also calculated as for Ibrahim's data. That is, these two data sets encompass the time range of 1 – 10000 s and the resuspension rate range of 10^{-8} – 10^{-1} s^{-1} (Figure 4).

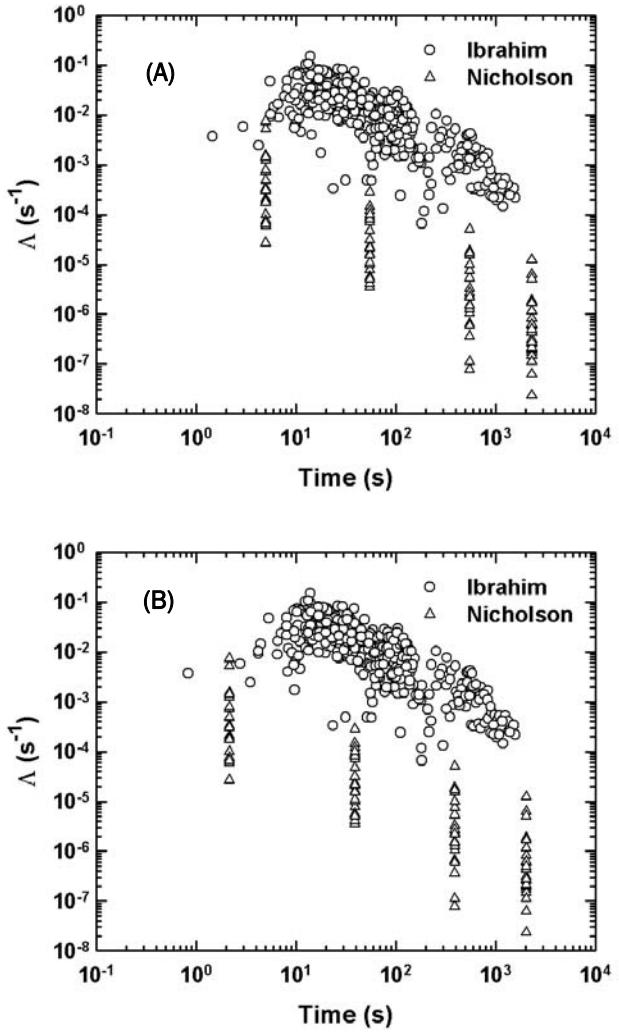

Figure 4. Resuspension rate versus time plotted from the data of Ibrahim (2004) and Nicholson (1993). For the corresponding time, (a) used the mid-point and (b) used t' defined by Eq 45.

The Hamaker constants for Ibrahim's and Nicholson's data were calculated using Equation 4. For example, to calculate the Hamaker constant for stainless steel (particle)-glass (surface)-air (medium), the Hamaker constants for stainless steel-stainless steel-air (vacuum) and glass-glass-air (vacuum) are needed.

Table 3 lists the Hamaker constants for homogenous substances that were used for Equation 4. The Hamaker constant for stainless steel-stainless steel-vacuum was assumed to be the same as that of steel-steel-vacuum. The Hamaker constant for Lycopodium-Lycopodium-air was calculated using Equation 4 and the Hamaker constants for Lactobacillus-glass-water, water-water-air, and glass-glass-air, assuming that biological materials have similar values for the Hamaker constant since the molecular compositions are similar. Under the same assumption, the value of the Hamaker constant for grass-grass-vacuum was considered as the same as that of Lycopodium-Lycopodium-air once obtained. The Hamaker constant for concrete-concrete-air is not available, and it was assumed to be 5×10^{-20} J.

3.3.1.2 Effect of RH

As mentioned earlier, Ibrahim's data were the most extensive with variations in relative humidity, particle sizes, densities, and materials. Table 4 briefly lists experimental data from Ibrahim (2004); and SS70 was used in the most of experiments. If all the results using SS70 are pooled (Figures 5.2, 5.3, 5.4, 5.7, 5.9, and 8.1 from Ibrahim [2004]), the particle size, the density, and materials for particle and surface are constant for these data sets. Variables for these experiments are RH, the acceleration, and the final free stream velocity.

Table 3. Hamaker constants used for calculating A_{132} for Ibrahim's and Nicholson's data.

Material	A (J)	Reference
steel-steel-vacuum	21.2×10^{-20}	Soltani and Ahmadi (2004)
glass-glass-dry air	8.5×10^{-20}	Soltani and Ahmadi (2004)
SiO_2-SiO_2-vacuum	6.82×10^{-20}	French (2000)
Lycopodium-Lycopodium-air	6.5×10^{-20}	Calculated from Lactobacillus-glass-water (6.2×10^{-21} J, Rijnaarts et al. (1995)), water-water-air (3.7×10^{-20} J), and glass-glass-air
grass-grass –air	6.5×10^{-20}	Assumed to be the same as Lycopodium-Lycopodium-air
concrete-concrete-air	5×10^{-20}	Assumed

Table 4. Variables for the experimental work by Ibrahim (2004).

Figure No. from Ibrahim 2004	Particle	Particle Density (kg/m^3)	Surface	T (°C)	Acceleration (m/s^2)	Initial Particle No. Density (mm^{-2})	RH (%)	
5.2	SS70	8000	Glass	23	0.18	0.5	Varied	Effect of RH
5.3	SS70	8000	Glass	23	Varied	0.5	36	Effect of acceleration
5.4	SS70	8000	Glass	23	Varied	0.5	61	Effect of acceleration
5.7	SS70	8000	Glass	23	0.18	0.5	30	Effect of final free stream velocity
5.9	SS70	8000	Glass	23	0.15	0.5	25	Variability of results for the same experimental condition
6.2	GL72 GL32	2420	Glass	23	0.18	0.5	25	Effect of particle size
6.5	GL32 LY30	2420 1000	Glass	23	0.15	0.5	25	Effect of particle density
8.1	SS70	1000	Glass	23	0.014	0.5	52	Variability of results for the same experimental condition

The final free stream velocity did not affect the fraction of particle resuspended, as noted by the author, and can be eliminated from the variables. In contrast, the flow acceleration during the transient period did have an effect on the fraction of particle resuspended. However, the acceleration is not the parameter considered here for resuspension, and it was decided to neglect the effect of the flow acceleration. Consequently, the pooled data for SS70 has only one variable (RH). Note that the data that were duplicated among Ibrahim's figures were deleted while being pooled.

For the pooled data with SS70, the particle size, the particle density, the surface roughness length, and the Hamaker constant were constant. Then, Equation 39 can be simplified further to for these pooled data as:

$$\Lambda = f(t, u_*, \mathrm{RH}, \rho_a) \qquad \text{Eq 46}$$

And, the resulting dimensionless variables are:

$$\frac{\Lambda d_p}{u_*} = f\left(\frac{u_* t}{d_p}, \mathrm{RH}\right) \qquad \text{Eq 47}$$

Assuming a power law for each variable, Equation 47 becomes:

$$\frac{\Lambda d_{\mathrm{p}}}{u_*} = a0\left(\frac{u_* t}{d_{\mathrm{p}}}\right)^{a1}\left(1 + a2 \cdot \mathrm{RH}^{a3}\right) \qquad \text{Eq 48}$$

It can also be expressed as:

$$\ln\left(\frac{\Lambda d_{\mathrm{p}}}{u_*}\right) = \ln(a0) + a1 \cdot \ln\left(\frac{u_* t}{d_{\mathrm{p}}}\right) + \ln\left(1 + a2 \cdot \mathrm{RH}^{a3}\right) \qquad \text{Eq 49}$$

Equation 49 implies that the plot of $\ln(\Lambda d_{\mathrm{p}}/u_*)$ vs. $\ln(u_* t/d_{\mathrm{p}})$ at a specific RH is a straight line and the slope is $a1$. In addition, the slope does not change at different RH, but the intercept does.

Figure 5 shows the graph of $\ln(\Lambda d_{\mathrm{p}}/u_*)$ vs. $\ln(u_* t/d_{\mathrm{p}})$ at various RH. Most of the data form a cluster around what could be a straight line with some scatter regardless of RH. Moreover, the scatter is not confined to a certain RH, but is noticeable from all RH. This graph does not illustrate that different intercepts are needed for different values of RH, and does indicate that the effect of RH is rather small and can be neglected in the range of 18 – 67 percent. Therefore, it was decided to exclude the RH from the relevant parameters in Equations 39, 41, and 43.

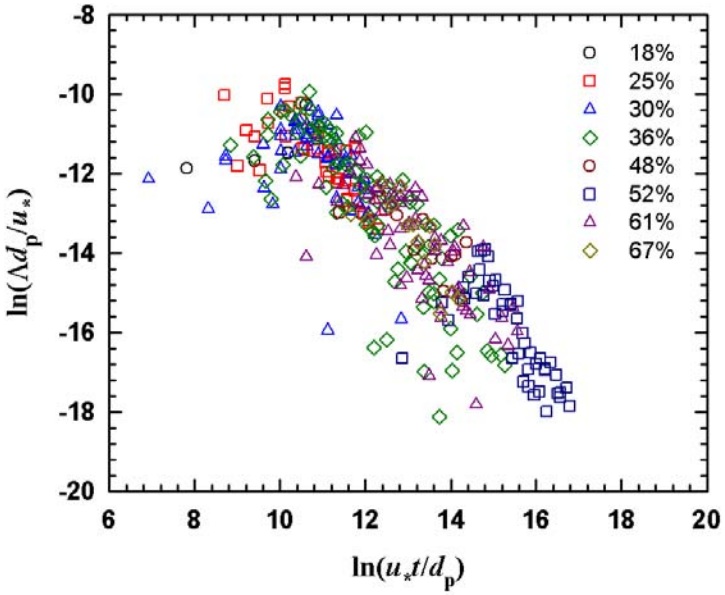

Figure 5. Plot of $\ln(\Lambda d_{\mathrm{p}}/u_*)$ vs. $\ln(u_* t/d_{\mathrm{p}})$ of all SS70 results with different RH from Ibrahim (2004).

3.3.1.3 Empirical Correlations

If one assumes that a power law applies for each dimensionless number in Equation 40 and the effect of RH is negligible, then a general correlation can be expressed as:

$$\frac{\Lambda d_{\mathrm{p}}}{u_*} = b0\left(\frac{\rho_{\mathrm{p}}}{\rho_{\mathrm{a}}}\right)^{b1}\left(\frac{u_* t}{d_{\mathrm{p}}}\right)^{b2}\left(\frac{z_0}{d_{\mathrm{p}}}\right)^{b3}\left(\frac{A_{132}}{d_{\mathrm{p}}{}^3 u_*{}^2 \rho_{\mathrm{a}}}\right)^{b4} \quad \text{Eq 50}$$

Taking the logarithms of both sides yields:

$$\ln\left(\frac{\Lambda d_{\mathrm{p}}}{u_*}\right) = \ln(b0) + b1\cdot\ln\left(\frac{\rho_{\mathrm{p}}}{\rho_{\mathrm{a}}}\right) + b2\cdot\ln\left(\frac{u_* t}{d_{\mathrm{p}}}\right) + b3\cdot\ln\left(\frac{z_0}{d_{\mathrm{p}}}\right) + b4\cdot\ln\left(\frac{A_{132}}{d_{\mathrm{p}}{}^3 u_*{}^2 \rho_{\mathrm{a}}}\right) \quad \text{Eq 51}$$

To obtain the coefficients $b0$–$b5$, a multiple regression was done using Ibrahim's and Nicholson's data with the mid-point as the corresponding time for the resuspension rate. Table 5 lists the results of a multiple regression, and the correlation becomes:

$$\frac{\Lambda d_{\mathrm{p}}}{u_*} = 8.521\times10^{-3}\left(\frac{\rho_{\mathrm{p}}}{\rho_{\mathrm{a}}}\right)^{-0.3028}\left(\frac{u_* t}{d_{\mathrm{p}}}\right)^{-1.0135}\left(\frac{z_0}{d_{\mathrm{p}}}\right)^{-0.3269}\left(\frac{A_{132}}{d_{\mathrm{p}}{}^3 u_*{}^2 \rho_{\mathrm{a}}}\right)^{-0.2961} \quad \text{Eq 52}$$

Table 5. The multiple regression result of Eq 51 using Ibrahim's (2004) and Nicholson's (1993) data with the mid-point as the corresponding time for the resuspension rate.

R = 0.96046136 R^2= 0.92248603 Adjusted R^2 = 0.92190540 Standard Error of Estimate = 1.0451					
	Coefficient	Standard Error	*t*	P	
ln(*b*0)	-4.7652	0.7346	-6.4865	<0.0001	
*b*1	-0.3028	0.0855	-3.5397	0.0004	
*b*2	-1.0135	0.0263	-38.5816	<0.0001	
*b*3	-0.3269	0.0200	-16.3183	<0.0001	
*b*4	-0.2961	0.0383	-7.7326	<0.0001	
Analysis of Variance:					
	DF	SS	MS	F	P
Regression	4	6941.3353	1735.3338	1588.7701	<0.0001
Residual	534	583.2612.3711	1.0922		
Total	538	7524.5967	13.9862		

The R^2 value for the correlation is 0.92, and the probabilities for any coefficient to be zero is very low (<0.0001 – 0.0004). The exponent for the t term is -1.0145, consistent with the findings of Nicholson (1993) and Loosmore (2003).

The same procedures were used to derive empirical correlations, denoted EC I to EC VII, for different groups of dimensionless variables in Cases 2 through 4 (Sections 3.2.2–3.2.4, pp 16–17) while assuming the effect of RH on the resuspension rate was negligible. Each dimensionless function was evaluated using both the mid-point and t' for the corresponding time for the resuspension rate; Table 6 lists the results. Although all the statistics of each multiple regression are not shown, the probability of the F-test was <0.0001 for all empirical correlations. The probabilities for any coefficient to be zero from the two-tailed t-test were also very low; in most of cases p<0.0001 and in all cases p<0.05 except for EC VI. In EC VI, p from the t-test for ln($d0$) and $d4$ was 0.2387 and 0.0713, respectively. Therefore, EC VI was re-evaluated while letting ln(d0) = 0 and $d4$ = 0; the resulting correlation is shown as EC VII (which does not contain the Hamaker constant as a variable).

The data listed in Table 6 show that, for the same group of dimensionless numbers, choosing either the mid-point or t' as the representative time for the resuspension did not affect the results of empirical correlations significantly; the exponents for each dimensionless parameter are similar and R^2 values are changed little. A better fit was expected using t' as the corresponding time for the resuspension, but the mid-point time showed very slightly better fits for all three different groups of dimensionless numbers.

The empirical correlations (EC I – EC VII) were non-dimensionalized to examine the dependency of Λ on the variables; Table 7 lists the results. For all empirical correlations, the exponent of the time term is between -0.92 and -1.04; these values are similar to those in Loosmore's work (2003) or the findings by Nicholson (1993). All these correlations suggest that Λ increases with u^* to the power n with n<1, and this is smaller than that suggested by Loosmore. Sehmel also noted that the air concentration is found to increase with wind speed to power n, with n between 1 and 6.42 (Rijnaarts et al. 1995). Therefore, the exponents for u^* in the correlations here seem too low compared to values reported in the literature. On the other hand, the dependency on the particle diameter in these correlations is stronger than that of Loosmore (2003).

Table 6. Empirical correlations obtained using different groups of dimensionless numbers. Each dimensionless function was evaluated using both the mid-point and *t′* for the time that represents the resuspension rate, and the effect of the RH was assumed to be negligible.

	with mid-point	with *t′*
From Equation 40 $\frac{\Lambda d_p}{u_*} = b0\left(\frac{\rho_p}{\rho_a}\right)^{b1}\left(\frac{u_* t}{d_p}\right)^{b2}\left(\frac{z_0}{d_p}\right)^{b3}\left(\frac{A_{132}}{d_p{}^3 u_*{}^2 \rho_a}\right)^{b4}$	EC I $b0$ = 8.521×10^{-3} $b1$ = -0.3028 b2 = -1.0135 b3 = -0.3269 b4 = -0.2961 R^2 = 0.9224	EC IV $b0$ =3.753×10-3 b1 = -0.2921 b2 = -0.9712 b3 = -0.3646 b4 = -0.2820 R^2 = 0.9215
From Equation 42 $\frac{\Lambda d_p}{u_*} = c0\left(\frac{u_* t}{d_p}\right)^{c1}\left(\frac{z_0}{d_p}\right)^{c2}\left(\frac{A_{132}}{d_p{}^3 u_*{}^2 \rho_p}\right)^{c3}$	EC II $c0$ = 3.708×10-4 c1 = -0.9635 c2 = -0.3224 c3 = -0.1742 R^2 = 0.9172	EC V $c0$ =1.882×10-4 c1 = -0.9255 c2 = -0.3576 c3 = -0.1672 R^2 = 0.9158
From Equation 44 $\frac{\Lambda d_p}{u_*} = d0\left(\frac{\rho_p}{\rho_a}\right)^{d1}\left(\frac{u_* t}{d_p}\right)^{d2}\left(\frac{z_0}{d_p}\right)^{d3}\left(\frac{A_{132}}{d_p{}^3 u_*{}^2 \rho_a}\right)^{d4}\left(\frac{\mu_a}{d_p u_* \rho_a}\right)^{d5}$	EC III $d0$ = 5.193×102 d1 = -0.4096 d2 = -1.0959 d3 = -0.3408 d4 = 0.4815 d5 = -1.8636 R^2 = 0.9249	EC VI $d0$ = 2.509×101 d1 = -0.3761 d2 = -1.0336 d3 = -0.3791 d4 = 0.3468 d5 = -1.500 R^2 = 0.9231 EC VII d0 = 1 d1 = -0.4644 d2 = -1.0352 d3 = -0.3649 d4 = 0 d5 = -0.7861 R^2 = 0.9221

Table 7. Dependency of Λ on each variable for different models.

Model	Exponent of							
	t	u_*	d_p	ρ_p	z_0	A_{132}	ρ_a	μ_a
EC I	-1.0135	0.5787	1.2311	-0.3028	-0.3269	-0.2961	0.5989	—
EC II	-0.9635	0.3849	0.8085	0.1742	-0.3224	-0.1742	—	—
EC III	-1.0959	0.8047	0.8558	-0.4096	-0.3408	0.4815	1.7917	-1.8636
EC IV	-0.9712	0.5928	1.1818	-0.2921	-0.3646	-0.2820	0.5741	—
EC V	-0.9255	0.4089	0.7847	0.1672	-0.3576	-0.1672	—	—
EC VI	-1.0336	0.7728	0.8723	-0.3761	-0.3791	0.3468	1.5293	-1.5000
EC VII	-1.0352	0.7509	1.1862	-0.4644	-0.3649	—	1.2505	-0.7861
Eq 28*	-0.92	2.13	0.17	-0.76	-0.32	—	—	—
Eq 29 *	-1.03	1.43	—	—	—	—	—	—
* from Loosmore (2003)								

EC I and EC IV illustrate that Λ increases with increasing u_* and d_p and decreases with increasing t, ρ_p, and z_o. This is consistent with the findings by others, and the reasoning for these dependencies is described in Section 2.3 (p 13) and can also be found elsewhere (Loosmore 2003). In addition, EC I and EC IV also implied that Λ increases with decreasing A_{132} and increasing ρ_a. The lower value of the Hamaker constant implies that the van der Waals forces between particles and surfaces are smaller, and thus the particles can be easily resuspended. The higher value of air density would increase the forces from the flow to the particles and increase the resuspension rate.

EC II and EC V were the correlations using the dimensionless numbers in Equation 40, where ρ_a was eliminated from the relevant parameters. These two correlations indicate that the resuspension rate increases with increasing particle density. Loosmore noted that the gravitational attraction is expected to be much smaller than the van der Waals or capillary adhesion forces and, therefore, the particle density is not believed to affect the resuspension rate directly (Loosmore 2003). However, the author also mentioned that deposition or re-deposition after resuspension depends strongly on particle mass and, thus, particle density. Therefore, particles with a higher density would result in a lower net resuspension rate for the same size particles, which is the opposite of predictions by EC II and EC V. Since they render physically unrealistic models, EC II and EC V are not considered further.

EC III and EC VI include μ_a as a parameter and suggest that the resuspension rate increases with decreasing the fluid viscosity or increasing Re. Although this is reasonable, the models also indicate that the resuspension rate increases as the Hamaker constant increases. A higher Hamaker constant means higher van der Waals adhesion and should result in a lower resuspension rate. Therefore, EC III and EC VI do not make physical sense and are not considered further.

In summary, only EC I, EC IV, and EC VII (which does not include the Hamaker constant as a variable) are acceptable.

3.3.2 Physics-Based Model

A physics-based model was also developed using a moment balance between adhesion and removal. According to literature, the most realistic way of particle resuspension is by rolling or tangential lift. Therefore, the condition for particle detachment was assumed to be when the removal

moment is bigger than the adhesion moment. In another words, if the moment ratio, M, is defined as:

$$M = \frac{\text{Adhesion Moment}}{\text{Removal Moment}} \quad \text{Eq 53}$$

then M<1 is the resuspension condition. For the adhesion force, using the Johnson-Kandall-Roberts (JKR) model (Johnson et al. 1971), the adhesion moment is expressed as:

$$M_a = \frac{3}{2}\pi r_{\mathrm{p}}\sigma \cdot r_{\mathrm{a}} \quad \text{Eq 54}$$

Here, r_{p} is the particle radius, σ is the surface energy, and r_{a} is the contact radius. The hydrodynamic removal moment is from the drag force, and therefore:

$$M_r = 1.4 F_D r_{\mathrm{p}} \quad \text{Eq 55}$$

and

$$F_D = 6\pi\mu_{\mathrm{a}}\dot{\gamma}\, r_{\mathrm{p}}^2 f \quad \text{Eq 56}$$

Here, $\dot{\gamma}$ is the shear rate and f = 1.7009. Because the friction velocity and the shear rate are related as:

$$u_* = \left(\frac{\tau_{\mathrm{w}}}{\rho_{\mathrm{a}}}\right)^{1/2} = \left(\frac{\mu_{\mathrm{a}}\dot{\gamma}}{\rho_{\mathrm{a}}}\right)^{1/2} \quad \text{Eq 57}$$

Equation 53 becomes:

$$M = \frac{1}{5.6 f}\frac{\sigma r_{\mathrm{a}}}{u_*^2 \rho_{\mathrm{a}} r_{\mathrm{p}}^2} \quad \text{Eq 58}$$

and Equation 58 can be rearranged with two dimensionless numbers as:

$$M = \frac{1}{5.6 f}\left(\frac{\sigma}{u_*^2 \rho_{\mathrm{a}} r_{\mathrm{p}}}\right)\left(\frac{r_{\mathrm{a}}}{r_{\mathrm{p}}}\right) \quad \text{Eq 59}$$

or with thee dimensionless numbers as:

$$M = \frac{1}{5.6f}\left(\frac{\sigma}{u_*^2 \rho_p r_p}\right)\left(\frac{r_a}{r_p}\right)\left(\frac{\rho_p}{\rho_a}\right) \quad \text{Eq 60}$$

The contact radius, r_a, at the moment of separation is given by:

$$r_a = \frac{r_{a0}}{4^{1/3}} \quad \text{Eq 61}$$

where r_{ao} is the contact radius at zero applied load given as:

$$r_{a0} = \left(\frac{6\pi r_p^2 \sigma}{K}\right)^{1/3} \quad \text{Eq 62}$$

and

$$K = \frac{4}{3}\left[\frac{1-\nu_1^2}{E_1} + \frac{1-\nu_2^2}{E_2}\right]^{-1} \quad \text{Eq 63}$$

Here, E_1 and E_2 are Young's moduli for the particle and the surface, respectively, and ν_1 and ν_2 are Poisson ratios of the particle and the surface, respectively. The resuspension rate, Λ, is defined as:

$$\Lambda = -\frac{1}{N_0}\frac{dN}{dt} \quad \text{Eq 64}$$

where:

N_0 and N are the number density of particles on the surface at time 0 and t, respectively.

Wen and Kasper (1989) assumed a Langmuir model for the particle desorption kinetics. Using the same assumption:

$$N = N_0 e^{-at} \quad \text{Eq 65}$$

and the rate constant a is a function of M.

According to Wen and Kasper, a requirement for $a(M)$ is to decrease with increasing M. The two simplest functions that meet the requirement are:

$$a = A_1 e^{-M} \quad \text{Eq 66}$$

and

$$a = \frac{A_2}{M} \quad \text{Eq 67}$$

By choosing Equation 66, Equation 64 can be rewritten as:

$$\Lambda = A_1 e^{-M} \cdot e^{-A_1 e^{-M} t} \quad \text{Eq 68}$$

By introducing the definition:

$$\tau_1 = \frac{e^M}{A_1} \quad \text{Eq 69}$$

and rearranging Equation 65, one obtains:

$$\Lambda = \frac{1}{\tau_1} e^{-t/\tau_1} \quad \text{Eq 70}$$

Alternatively, choosing Equation 67 results in:

$$\Lambda = \frac{1}{\tau_2} e^{-t/\tau_2} \quad \text{Eq 71}$$

with:

$$\tau_2 = \frac{M}{A_2} \quad \text{Eq 72}$$

For given particles, M is a constant. Therefore, a model can be obtained by fitting Equation 70 or 71 to experimental data to find A_1 or A_2, respectively.

3.3.3 Comparison of Dimensionless Variables in Empirical Correlations and Physics-based Model

One of the motivations for developing a physics-based model was to determine dimensionless variables that are based on physics and examine whether they can be used for drawing empirical correlations. The dimensionless numbers from the physics-based model in Equation 59 were compared to those used for empirical correlations in Equation 40. In Equation 59, two dimensionless numbers take account for the properties of particles and surfaces: $\sigma/u_*^2\rho_a r_p$ and r_a/r_p. In Equation 40, the term with the Hamaker constant ($A_{132}/d_p^3 u_*^2 \rho_a$) takes into account the material

characteristics of particles and surfaces. If the "contact" interaction from the JKR model is used instead of the van der Waals interaction for the empirical correlations, then Equation 40 can be replaced with:

$$\frac{\Lambda d_{\mathrm{p}}}{u_*} = f\left(\frac{\rho_{\mathrm{p}}}{\rho_{\mathrm{a}}},\ \frac{u_* t}{d_{\mathrm{p}}},\ \mathrm{RH},\ \frac{z_0}{d_{\mathrm{p}}},\ \frac{\sigma}{u_*{}^2 \rho_{\mathrm{a}} d_{\mathrm{p}}},\frac{d_{\mathrm{a}}}{d_{\mathrm{p}}}\right) \qquad \text{Eq 73}$$

Here, d_{a} is the contact diameter, $2r_{\mathrm{a}}$. Acquiring an empirical correlation with the dimensionless numbers in Equation 73 will be pursued in Phase II of this project.

3.4 Testing of Models

Empirical correlations, EC I, EC IV, and EC VII, were compared against the experimental results by Giess et al. (1977), Braaten et al. (1990), Wu et al. (1992), Krauter and Biermann (2007), and Wen and Kasper (1989).

3.4.1 Collected Experimental Data

Figure 6 shows the data from the literature to test empirical correlations; Tables 8 and 9 list their experimental parameters.

The friction velocity for the data by Wu et al. (1992) was calculated using the following equation for duct flows (suggested by Davies [1972]) and the free stream velocity:

$$u_* = \left(\frac{\nu}{d_{\mathrm{h}} U_\infty}\right)^{1/8} \frac{U_\infty}{5} \qquad \text{Eq 74}$$

where:

d_{h} = the hydraulic diameter.

Using work by Krauter and Biermann (2007) and Wen and Kasper (1989) the following equation for a pipe flow was used to calculate the friction velocity (Davies 1966):

$$u_* = \sqrt{\frac{f}{2}} U_\infty \qquad \text{Eq 75}$$

where:

f = the friction factor given by Blasius as:

$$f = \frac{0.3164}{4\,\mathrm{Re}^{0.25}} \qquad \text{Eq 76}$$

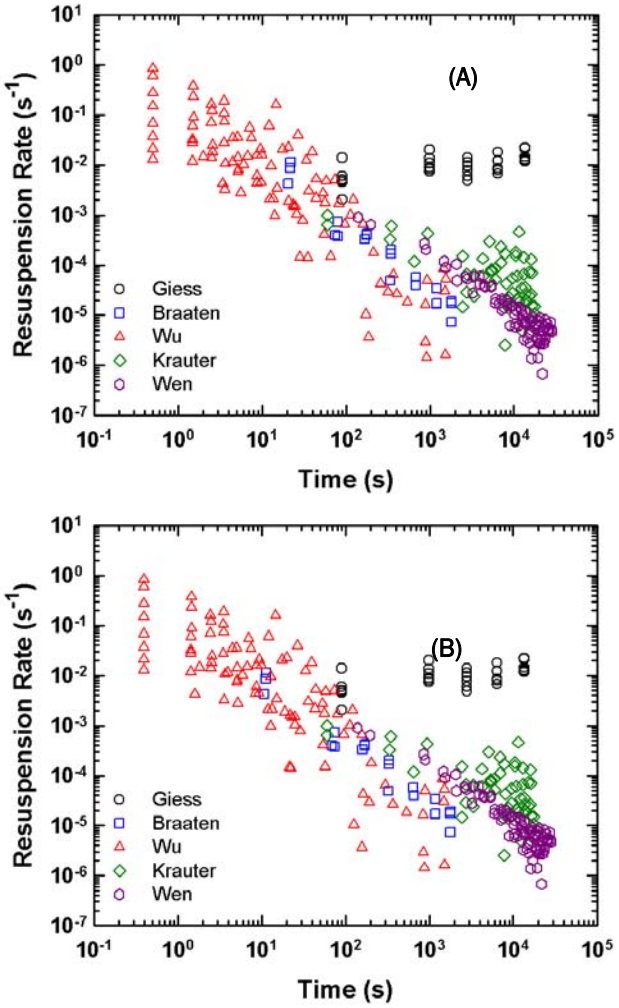

Figure 6. Resuspension rate versus time plotted from the data used to test empirical correlations. For the corresponding time, (A) used the mid-point and (B) used t' defined by Eq 45.

Table 8. Experimental parameters for works by Giess (1997) and Braaten (1990).

	Giess (1997)	Braaten (1990)
Dimensions for flow passage	Wind tunnel, 1.2 m × 0.8 m	Wind tunnel, 1 m × 1 m
Surface material	Grass	Glass
U_∞ (m/s)	3.0, 5.0, 7.8	6.0, 7.5, 9.0
u_* (m/s)	For short grass: 0.27, 0.64, 1.14 For long grass: 0.57, 0.75, 1.42	0.17, 0.215, 0.26
Particle	Silica spheres	Lycopodium spores
d_p (μm)	1.85	27.8
ρ_p (kg/m^3)	1000	1000
Surface feature height (m)	Short grass: 0.1 Long grass: 0.3	Not reported

	Giess (1997)	Braaten (1990)
Aerodynamic roughness (m)	Short grass: 0.01 Long grass: 0.03	1×10^{-6}: assumed by Loosmore (2003)
Temperature (°C)	Not reported, assumed to be 25	Not reported, assumed to be 25
RH (%)	Not reported	Not reported
Resuspension rate	Taken directly from Table 1	Computed from fraction loss of experimental data in Fig. 12 – Fig. 14
Number of data points	30	21

Table 9. Experimental parameters for works by Wu (1992), Krauter (2007), and Wen (1989).

	Wu (1992)	Krauter (2007)	Wen (1989)
Dimensions for flow passage	Wind tunnel, 1 m × 1 m	Round duct, D = 0.152 m	Capillary tubing, D = 0.125 cm
Surface material	Glass	Steel, plastic	Steel
U_∞ (m/s)	4, 6, 8	2.6	100
u_* (m/s)	0.169, 0.241, 0.310: calculated	0.144: calculated	5.16: calculated
Particle	Lycopodium spores	Bacillus atrophaeus spores	Latex particles
d_p (μm)	27.8	0.91	0.509, 1.019
ρ_p (kg/m^3)	1000	1200	1000
Surface feature height (m)	Not reported	Steel: 1.5×10^{-4}, plastic:5×10^{-6}	Not reported
Aerodynamic roughness (m)	1×10^{-6}: assumed by Loosmore[6]	Steel: 5×10^{-6}, plastic:1.67×10^{-7}	1×10^{-6}: assumed
Temperature (°C)	Not reported, assumed to be 25	Steel: 27, averaged Plastic: 24, averaged	22
RH (%)	Not reported	Steel: 26, averaged Plastic: 26, averaged	~ 0
Resuspension rate	Computed from the resuspension fraction from Fig. 4	Taken directly from Fig. 6	Computed from the particle concentration in air in Figs. 8 and 9
Number of data points	96	54	81
Other details			Pressure: 6 bar → ρ_a: 7.18 kg/m^3

The aerodynamic roughness for the data by Giess (1997) is assumed to be 1/10 of the physical roughness as discussed earlier. For the data by Braaten et al. (1990) and Wu et al. (1992), Loosmore assumed 1×10^{-6} m as the aerodynamic roughness for glass surfaces; it was decided to use the same value for this study. For reference, the aerodynamic roughness for glass surface used by Ibrahim's work was estimated as 4.1×10^{-9} m. As men-

tioned earlier, Krauter and Biermann (2007) estimated the aerodynamic roughness as 1/30 of the physical height of the surface; and values were used directly. The surface roughness for the steel capillary tubing used by Wen and Kasper (1989) was assumed to be 1×10^{-6} m.

The resuspension rates that were calculated from the resuspension fraction used the mid-point time as the corresponding time for EC I and t' for EC IV and EC VII for consistency. The resuspension rate of Wen and Kasper was computed from the particle concentration in air using the flow rate, the initial particle number density on the surface, and the surface area deposited with particles. Table 10 lists the homogenous Hamaker constants, in addition to those in Table 3, for the experimental data.

3.4.2 Model Testing

Figure 7 shows the ratio of the resuspension rate predicted by empirical correlations to the experimental results. The performances of the empirical correlations of EC I, EC IV, and EC VII were similar to all experimental data. For the data by Braaten et al. (1990) and Wu et al. (1992), the ratios of the predicted to the observed were mostly scattered between 0.1 and 10 for all three correlations. The ratios of the predicted to the observed by Wen and Kasper (1989) were distributed between 0.01 and 1 for EC I and EC IV. EC VII performed slightly better than EC I or EC IV for Wen and Kapser (1989), and this was the most distinguishable difference in comparison among the correlations. The ratio was relatively constant at ~0.01 for Giess et al. (1997), and the correlations greatly underestimated the data by Krauter and Biermann (2007).

Table 10. Additional Hamaker constants used for calculating A_{132} for Giess et al. (1997), Braaten et al. (1990), Wu et al. (1992), Krauter and Biermann (2007), and Wen and Kasper (1989).

Material	A (J)	Reference
B. atrophaeus-B. atrophaeus-air	6.5×10^{-20}	Assumed the same as Lycopodium-Lycopodium-air
latex sphere-latex sphere-air	4×10^{-20}	Assumed
plastic-plastic-air	7.8×10^{-20}	Assumed the same as PVC-PVC-vacuum

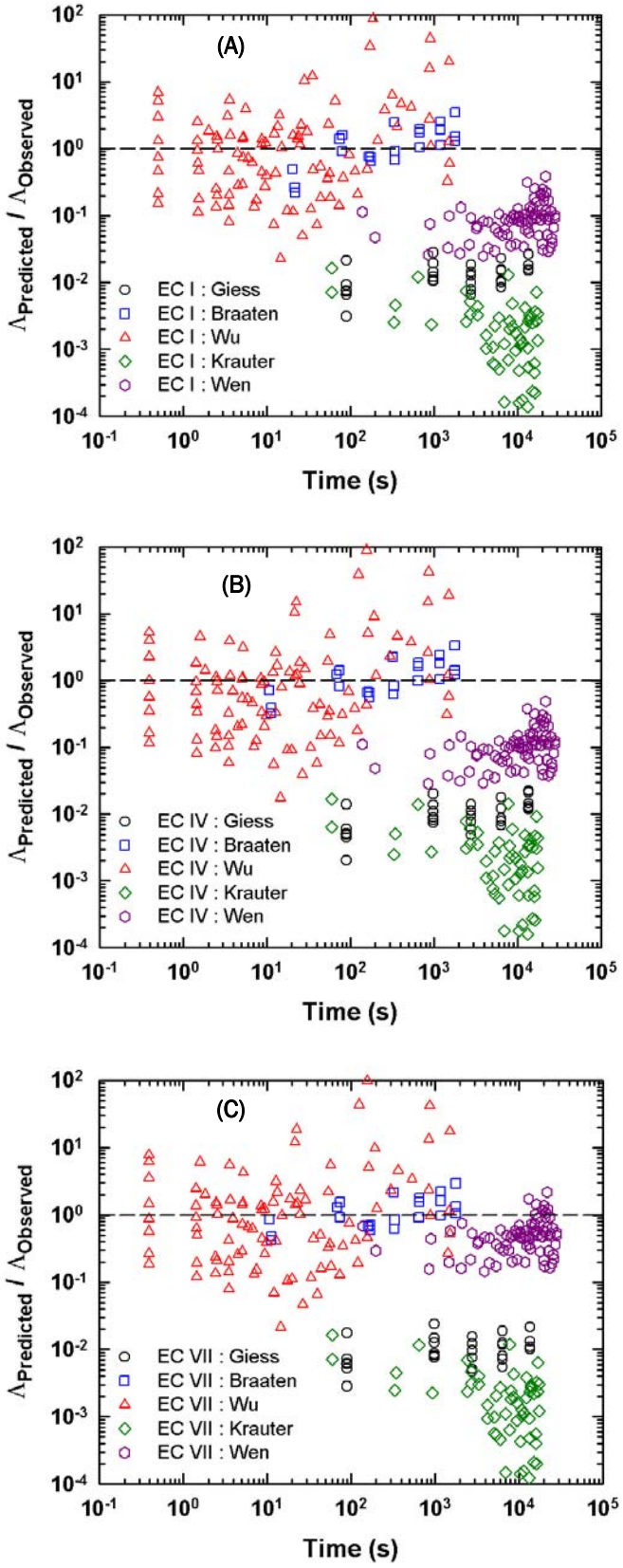

Figure 7. Performance of the empirical correlations, (A) EC I, (B) EC IV, and (C) EC VII, against experimental data.

Note that Loosmore's empirical correlations predicted the data by Braaten et al. (1990) and Wu et al. (1992) reasonably well (Loosmore 2003). The work by Wen and Kasper was done in a capillary tube with a very high free stream velocity (100 m/s); the data may not be comparable to others obtained with low velocities. Krauter and Biermann (2007) compared their experimental data to Loosmore's empirical correlation, and prediction by Loosmore's correlation was lower by two orders of magnitude than the experimental data. They also compared their data to those from the literature by adjusting for the friction velocity difference using the exponent for u^* in Loosmore's correlation. The resuspension rates from Braaten et al. and Wu et al. were an order of magnitude lower than those by Krauter and Biermann, and only the results by Wen and Kasper were comparable.

Because values for the surface roughness were not available for most of the experimental works, they were estimated to evaluate the empirical correlations. This can introduce or increase uncertainties in the empirical correlations. The correlations exponents for z_o were between –0.32 and –0.36. If the surface roughness would be 1/1000 of that specified in Table 8 and Table 9, it would cause an order of magnitude increase in the resuspension rate. Therefore, inaccurate estimation of the surface roughness would not affect the prediction of the resuspension rate too greatly.

The quality of an empirical correlation depends on the data used to draw the correlations, and some of the experimental details on the data by Ibrahim (2004), which was used in conjunction with the data by Nicholson (1993), deserve discussion. Specifically, Ibrahim's data were obtained using transient velocities compared to constant velocities used by most of the other works. In addition, some of Ibrahim's data were collected using very dense particles (ρ_p = 8000 kg/m^3). Since the empirical correlations were obtained using the dimensionless variables, some differences may have been scaled properly and the correlations can be valid for wide ranges of parameters. However, it may be possible that other differences may be fundamental, and empirical correlations derived from these data may not properly describe the resuspension data under different conditions. Therefore, to model and predict the indoor resuspension accurately it would be essential to derive models based on experimental data with the conditions that are characteristic to indoor resuspension.

Table 11 lists the results of simple sensitivity testing for the empirical correlations of EC I, EC IV, and EC VII. A factor-of-10 error in d_p would result in a factor of 15–17 change in the resuspension rate for all correlations. It is not likely to have a factor-of-10 error in the particle size, and the contribution from this error would be very small. An order of magnitude error in u_*, ρ_p, z_0, A_{132}, and ρ_a would cause only a factor of 2 – 4 change in Λ except for ρ_a in EC VII, and the contribution from the errors in these parameters would be limited.

Table 11. Sensitivity analyses of the empirical correlations of EC I, EC IV, and EC VII.

Factor-of-10 changes in the parameter of	Change in Λ		
	EC I	EC IV	EC VII
t	0.097	0.107	0.092
u_*	3.791	3.916	5.635
d_p	17.026	15.198	15.353
ρ_p	0.498	0.510	0.343
z_0	0.471	0.432	0.432
A_{132}	0.506	0.522	—
ρ_a	3.971	3.750	17.803
μ_a	—	—	0.164

4 Source Term Model for CFD Simulation

Demonstration simulations were performed using the empirical correlation EC I as a source term in a boundary condition for CFD simulations. The CFD simulations were based on the experiments performed by Lawrence Berkeley National Lab; a description of the experiments follows.

4.1 Description of Particle Resuspension in a Bench-top Test Chamber

A 30 in. (L) × 30 in. (W) × 36 in. (H) chamber was used for particle resuspension experiments. The chamber contained two, 3-blade muffin fans (blade span = 4.25 in., 115 V, 14 W, variable speed) mounted 10 in. from the floor and located in opposite corners of the chamber. The fans blew towards the center of the chamber, and the center of each fan was 6 in. from its respective corner (Figure 8). Make-up air at 20 L/min was introduced to the chamber from a 0.25 in. diameter port in the center of the right wall of the chamber, which was located 18 in. above the floor and 15 in. from the front wall and projected 0.25 in. into the chamber. An aerodynamic particle sizer (APS, Model 3321, TSI, Inc., St. Paul, MN) drew 5 L/min of air from a probe at the center of the floor. The probe extended 5.25 in. above the floor and had a 0.75 in. diameter. In addition, 10 L/min of air was sampled for filter measurement through a port 24 in. above the chamber floor and 10 in. from the front wall. It extended 5.75 in. into the chamber and had a 0.25-in. diameter. At 5 L/min, air leaked along the perimeters of 26 in. (W) × 32 in. (H) of a door on the front wall. Horizontal and vertical components of air velocity were measured using a hotwire anemometer at 9 points in a plane 10 cm above the floor specified in Figure 8.

During the particle deposition phase, the airborne particle concentration was measured with the APS, and the data collected by the APS were used to estimate the size distribution of particles deposited on the floor surfaces. During the particle resuspension phase, the airborne concentration was measured with both the APS and a filter sample. The resuspension phase for each experiment lasted 5 hrs, 1 hr with the fans off and 1 hr for each of four fan speeds (45, 75, 110, and 140). The fan speeds were incrementally increased each hour over the course of the experiment.

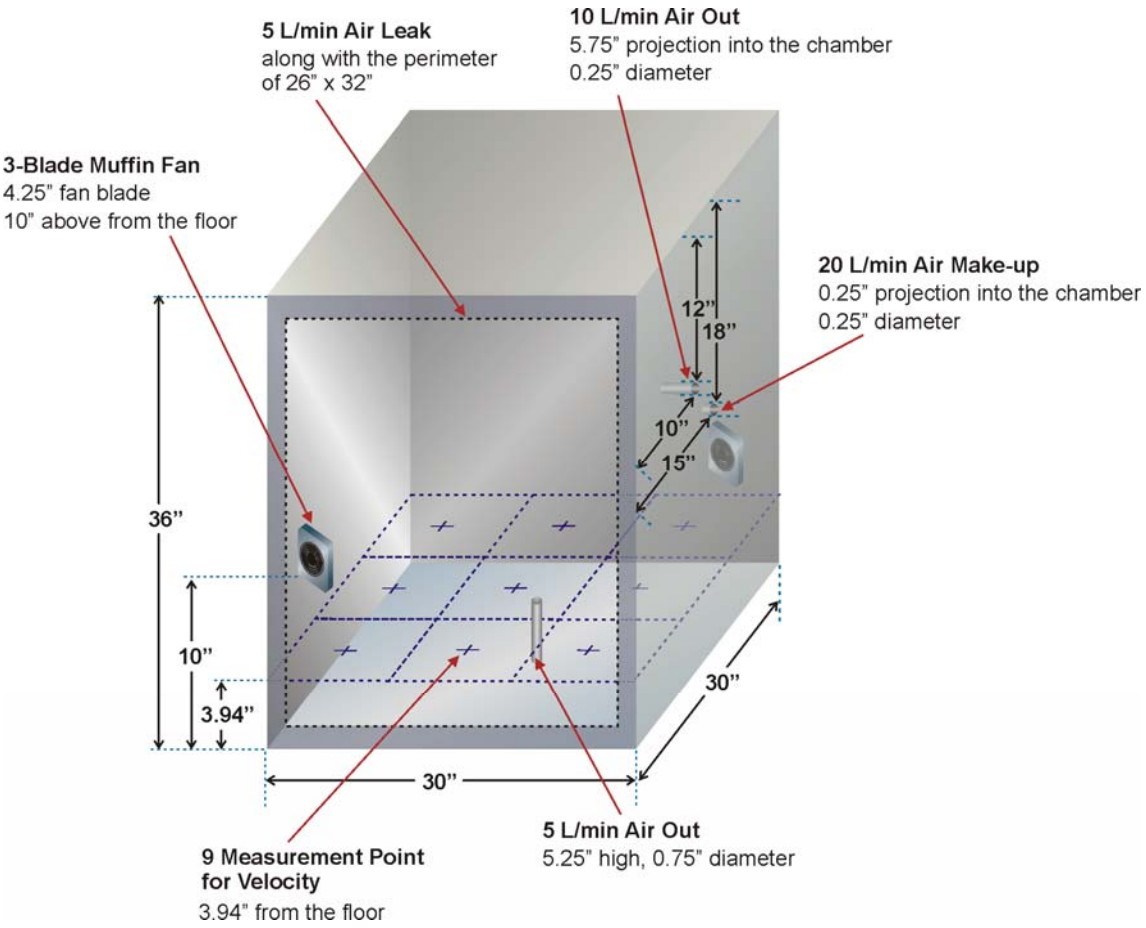

Figure 8. A schematic diagram of the chamber for particle resuspension experiments; all dimensions are in inches, and the x-y positions of the measurement points for velocity.

The floor of the chamber was completely covered with either moderately textured linoleum or commercial grade olefin carpet, and the sodium fluorescein powder was used as the particle.

4.2 CFD Simulations of Flow Field in the Test Chamber

4.2.1 Experimental Results

The data from the experiments that provided information on the flow field were the flow rate of the fans and the average horizontal and vertical velocities at the plane 10 cm above the floor; Tables 12, 13, and 14 list these values.

Table 12. Measured flow rates of the variable speed fan.

Fan Speed	Flow Rate (L/min)
45	6
75	20
110	40
140	70

Table 13. The average of the minimum, the average, and the maximum air velocity in the horizontal direction measured at the nine measurement points in the plane 10 cm above the floor for the four different fan speeds.

Fan Speed	Average of Minimums (cm/s)	Average of Averages (cm/s)	Average of Maximums (cm/s)
45	1.17	7.80	16.83
75	17.89	30.10	46.30
110	24.26	37.27	54.00
140	21.61	38.60	57.71

Table 14. The average of the minimum, the average, and the maximum air velocity in the vertical direction measured at the nine measurement points in the plane 10 cm above the floor for the four different fan speeds.

Fan Speed	Average of Minimums (cm/s)	Average of Averages (cm/s)	Average of Maximums (cm/s)
45	5.85	14.00	27.15
75	30.57	56.93	94.54
110	28.40	54.62	98.81
140	24.59	57.96	103.33

4.2.2 CFD Simulations of Flow Field

CFD simulations in this project were carried out in collaboration with CFD Research Corporation (Huntsville, AL). Based on the chamber geometry and flow conditions, a computational mesh was created using CFD-Micromesh, a mesh generation software developed and commercialized by CFDRC. Figure 9 shows model geometry and mesh distribution used in the simulations. Localized mesh refinement was used in regions where sharp flow gradients are expected, e.g., inlets, outlets, and regions affected by fan flow (Figure 9[B]). Three different mesh sizes were used to ensure mesh-independent results of flow field. A total of 45,113 grid-cells were used in the parametric study.

Once the mesh was generated, flow field was calculated inside the chamber based on the conditions provided using CFD code CFD-ACE+, originally developed by CFDRC and currently licensed by ESI Group (San Diego,

CA). Figure 10 shows the Graphical User Interface demonstrating the range of physical models available in CFD-ACE+. The "modules" that were used in the current simulation were "flow," "turbulence," and "user scalar." A "fan sub-model" was used for simulating flow and pressure head of the fan. The fans were assumed to have an outer radius of 5.2 cm and a hub radius of 2.975 cm.

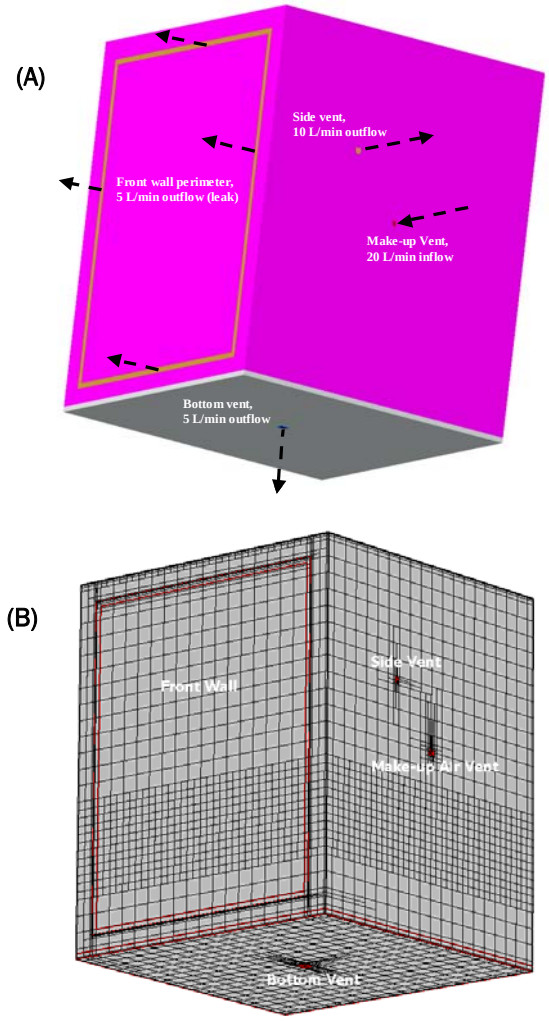

Figure 9. (A) 3D model of chamber showing the general direction of air flow through various inlets and outlets. (B) unstructured (binary-tree) mesh implemented inside the chamber 3D model. The refined mesh layer just below the make-up air vent is to resolve the flow modification through the two fans.

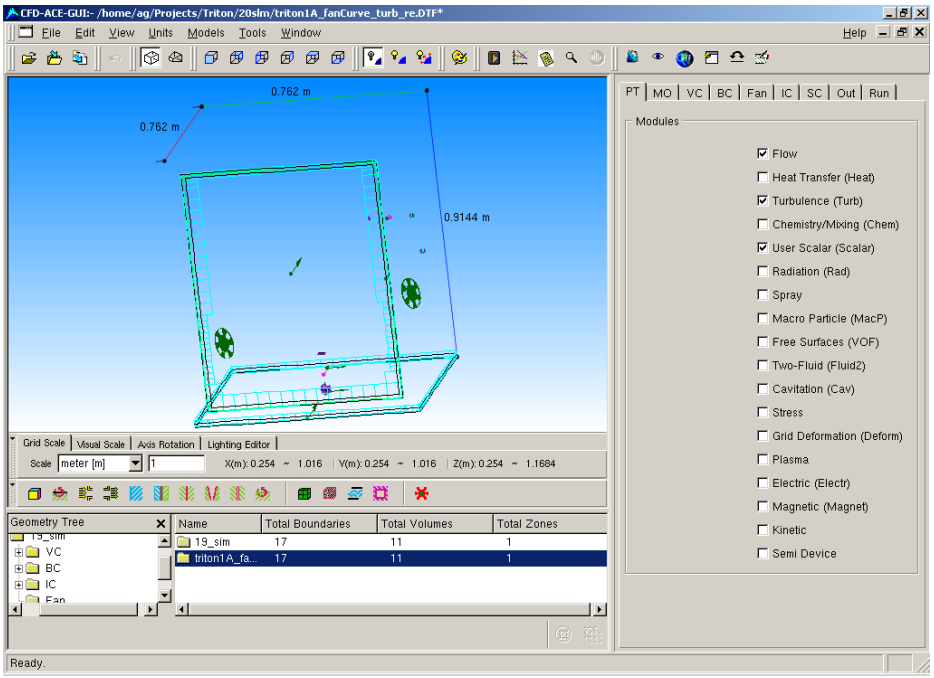

Figure 10. Snapshot of the CFD-ACE+ graphical user interface with physical models used in the simulations.

Parametric simulations of flow were performed for various fan flow rates. For comparison, Table 15 lists the measured and calculated fan flow rates, and the flow field generated by CFD simulations that could match the fan flow rates from the experiments. For reference, the average fan flow velocity was calculated based on the measured fan flow rate and the radius of the fan (either for the outer area or the hub area); the last two columns in Table 15 lists these values. Table 16 lists the average horizontal and vertical velocities of the nine points in the plane that was 10 cm above the floor. The measured average velocities were taken directly from Tables 13 and 14, and the calculated values were the results of CFD simulations of the flow field.

That data in Table 16 show that the average calculated velocities are significantly lower than measured values. Even when the flow rate was increased to 132.7 L/min, which was much higher than any of the experimental values, the average horizontal and vertical velocities were still considerably lower than any of experimental values. Because one could simply calculate the average fan flow velocity from the fan flow rate and the annulus area of the fan as shown in the last two columns in Table 15, researchers also examined the average horizontal and vertical velocities in the plane that contained the fans (Table 17). The average horizontal velocity in the plane 10 in. above the floor was slightly higher than the average fan flow velocity (in Table 15) for 6 – 40 L/min and lower for 70 and

132.7 L/min, but overall one could conclude that these two values agreed acceptably. Therefore, there seemed to be inconsistency between the measured flow rate and the measured average velocities. It was decided to use the measured fan flow rate for the basis of CFD simulation on particle resuspension.

Table 15. Measured and calculated fan flow rates; the average fan flow velocities were calculated from the measured fan flow rates from the experiments using the outer radius and the hub radius of the fans.

Measured Fan Flow Rate (L/min)	CFD Calculated Flow Rate for Fan #1 (L/min)	CFD Calculated Flow Rate for Fan #2 (L/min)	CFD Calculated Average Fan Flow Rate (L/min)	Average Fan Flow Velocity – Based on Outer Area (cm/s)	Average Fan Flow Velocity – Based on Annulus Area (cm/s)
6	6.56	6.40	6.48	1.18	1.75
20	20.36	19.48	19.92	3.92	5.83
40	40.39	36.76	38.57	7.85	11.67
70	61.68	55.16	58.42	25.51	37.91
—	150.36	115.08	132.7	33.31	49.52

Table 16. Measured and calculated average velocities of the nine measurement points in the plane 10 cm above the floor for various fan flow rates; the average horizontal and vertical velocities are from Tables 13 and 14.

Calculated (Measured) Fan Flow Rate (L/min)	Average Horizontal Velocity - Measured (cm/s)	Average Vertical Velocity - Measured (cm/s)	Average Horizontal Velocity - Calculated (cm/s)	Average Vertical Velocity - Calculated (cm/s)
6.48 (6)	7.80	14.00	5.03	3.61
19.92 (20)	30.10	56.93	4.50	4.14
38.57 (40)	37.27	54.62	4.10	3.76
58.42 (70)	38.60	57.96	4.60	4.06
132.7	—	—	9.79	7.41

Table 17. Measured and calculated average velocities of the nine points in the plane that the fans were placed (10 in. above the floor) for various fan flow rates; the x-y positions of the nine points were the same as those of the nine measurement points in Tbl. 16, but the z-positions for these points were 10-in from the floor instead of 10 cm.

Calculated (Specified) Fan Flow Rate (L/min)	Average Horizontal Velocity–Calculated (cm/s)	Average Vertical Velocity–Calculated (cm/s)
6.48 (6)	2.26	1.91
19.92 (20)	11.00	2.41
38.57 (40)	14.33	1.89
58.42 (70)	18.67	2.65
132.7	30.90	5.12

Figures 11–15 show the flow field and friction velocities in the chamber at a given fan flow rate. The flow field is plotted in the plane of the two fans as well as in the plane joining the fan centers (shown on the left). The figures on the right show isocontours of friction velocities at the floor of the chamber. As expected, as the fan flow rate is increased the velocities (including the friction velocities), and the turbulence levels in the chamber increase significantly.

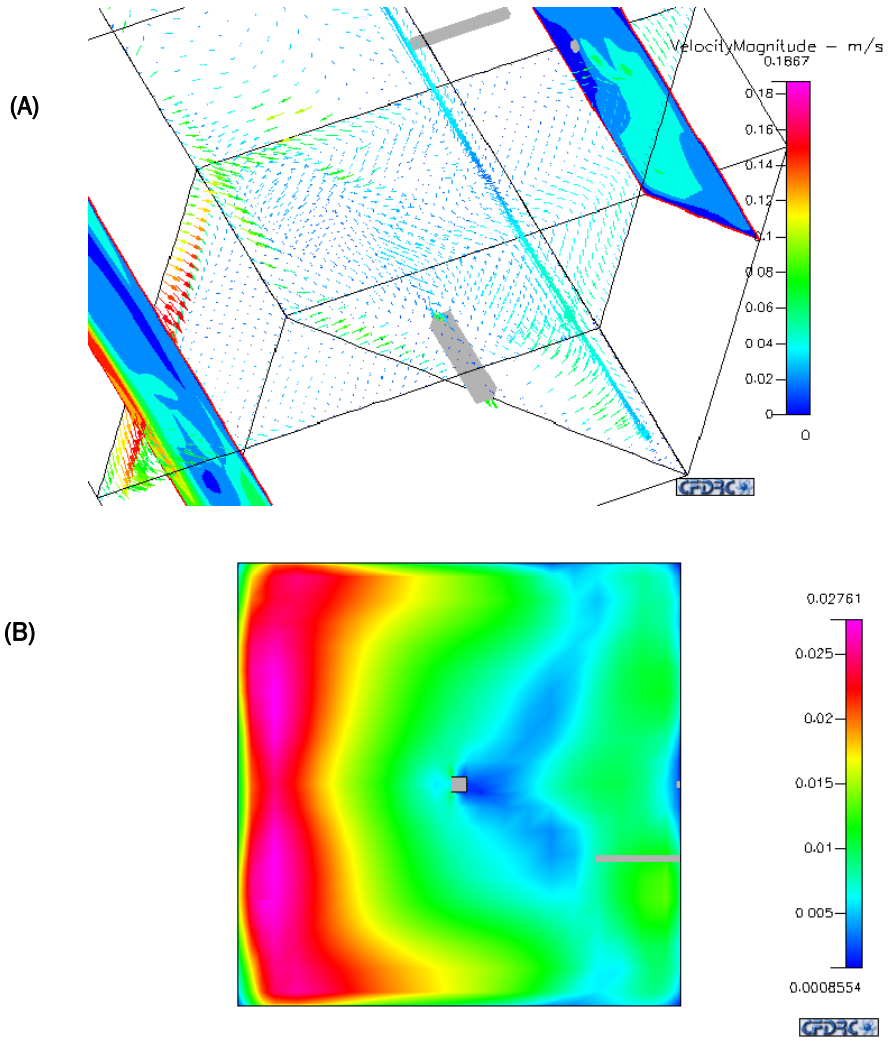

Figure 11. (A) Velocity vectors colored by magnitude of velocity in the plane through the fan centers; vectors are also plotted in the plane along the diagonal through bottom; isosurfaces of velocity magnitude in the plane of the two fans (6 L/min); (B) isocontours of the friction velocity at the floor (6 L/min).

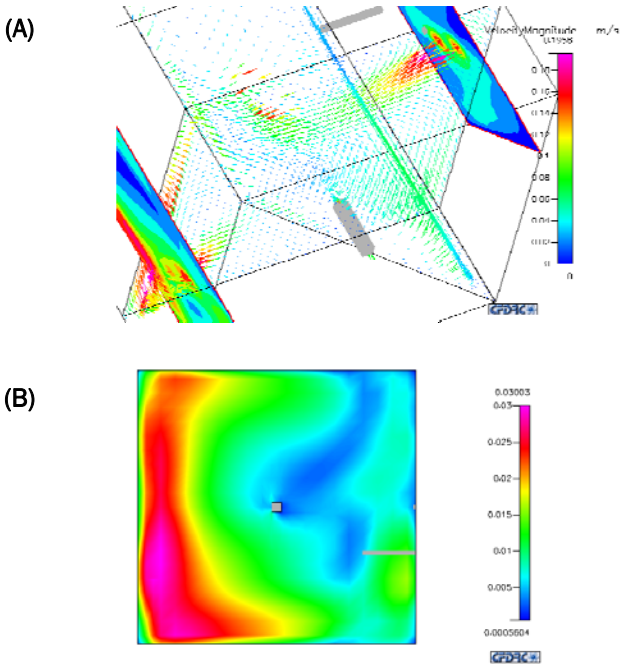

Figure 12. (A) Velocity vectors colored by magnitude of velocity in the plane through the fan centers; vectors are also plotted in the plane along the diagonal through bottom; isosurfaces of velocity magnitude in the plane of the two fans (20 L/min); (B) isocontours of the friction velocity at the floor (20 L/min).

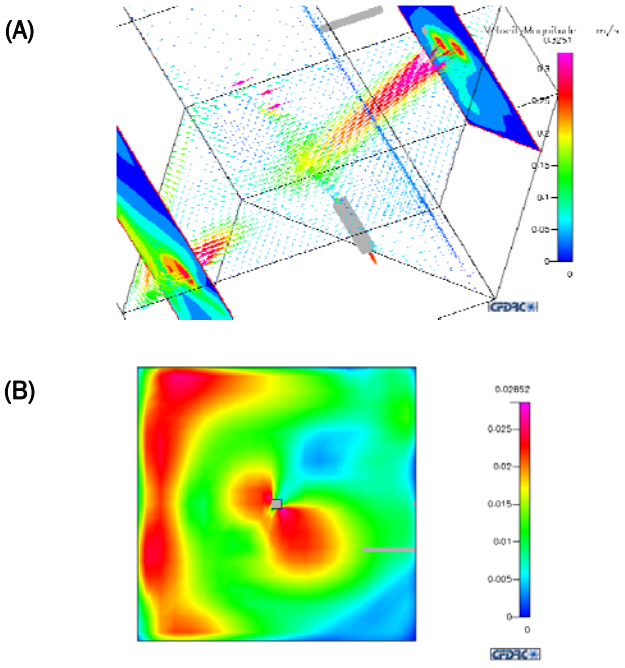

Figure 13. (A) Velocity vectors colored by magnitude of velocity in the plane through the fan centers; vectors are also plotted in the plane along the diagonal through bottom; isosurfaces of velocity magnitude in the plane of the two fans (40 L/min); (B) isocontours of the friction velocity at the floor (40 L/min).

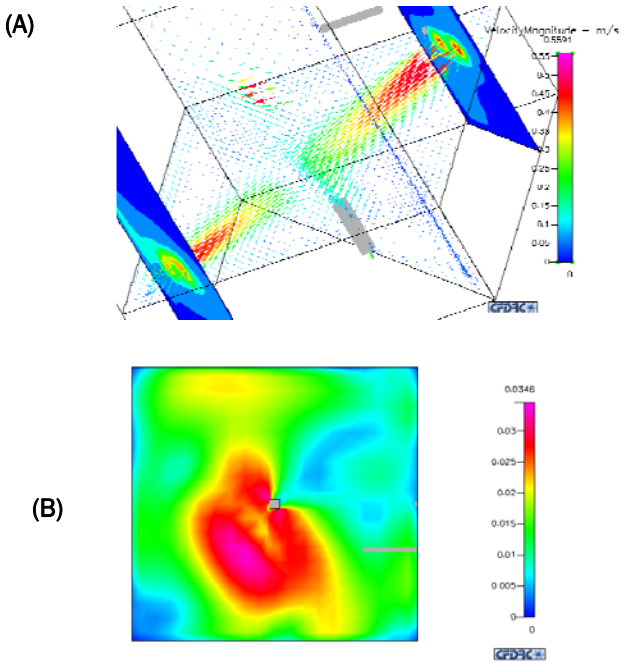

Figure 14. (A) Velocity vectors colored by magnitude of velocity in the plane through the fan centers; vectors are also plotted in the plane along the diagonal through bottom; isosurfaces of velocity magnitude in the plane of the two fans (60 L/min); (B) isocontours of the friction velocity at the floor (60 L/min).

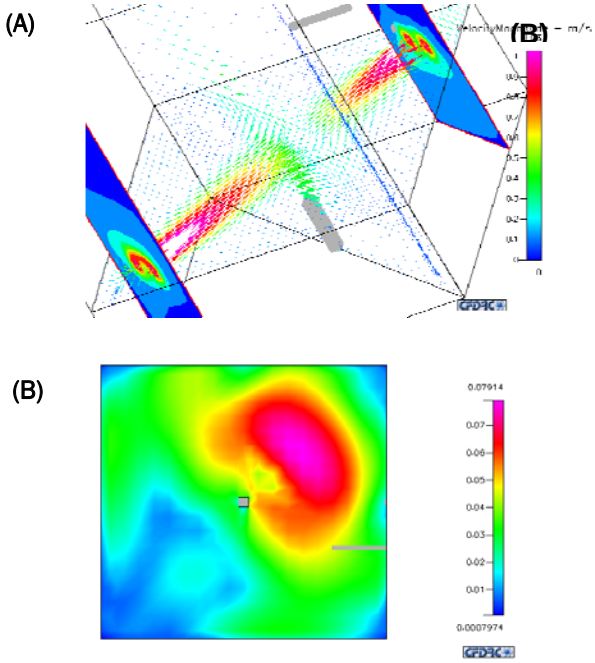

Figure 15. (A) Velocity vectors colored by magnitude of velocity in the plane through the fan centers; vectors are also plotted in the plane along the diagonal through bottom; isosurfaces of velocity magnitude in the plane of the two fans (132 L/min); (B) isocontours of the friction velocity at the floor (132 L/min).

4.3 CFD Simulation of Particle Resuspension and Transport

4.3.1 Resuspension Rate

As mentioned earlier, the empirical correlation EC I used as a source term in a boundary condition for CFD simulations is written as:

$$\frac{\Lambda d_{\mathrm{p}}}{u_*} = 8.521\times10^{-3}\left(\frac{\rho_{\mathrm{p}}}{\rho_{\mathrm{a}}}\right)^{-0.3028}\left(\frac{u_* t}{d_{\mathrm{p}}}\right)^{-1.0135}\left(\frac{z_0}{d_{\mathrm{p}}}\right)^{-0.3269}\left(\frac{A_{132}}{d_{\mathrm{p}}{}^{3} u_*{}^{2}\rho_{\mathrm{a}}}\right)^{-0.2961} \quad \text{Eq 77}$$

and, therefore, the resuspension rate is expressed as:

$$\Lambda = 8.521\times10^{-3}\frac{u_*{}^{0.5787} d_{\mathrm{p}}{}^{1.2311}\rho_{\mathrm{a}}{}^{0.5989}}{t^{1.0135}\rho_{\mathrm{p}}{}^{0.3028} z_0{}^{0.3269} A_{132}{}^{0.2961}} \quad \text{Eq 78}$$

In the experiments, the floor of the chamber was completely covered with either moderately textured linoleum or commercial grade short pile olefin carpet. Linoleum is made from solidified linseed oil (linoxyn) in combination with wood flour or cork dust over a burlap or canvas backing. A commercial grade olefin carpet is made of polypropylene, which is static resistant unlike nylon carpets. The physical roughness for linoleum and the short pile carpet were assumed to be 6.4 μm (Hallas and Shaw 2006) and 1 mm, respectively, and the aerodynamic surface roughness was taken as 1/10 of the physical roughness. The particle size distribution of the sodium fluorescein powder was measured using the APS, and it ranged between 0.5 – 15 μm. The density of the sodium fluorescein was 1.35 g/cm^3, and the density of air was 1.196×10^{-3} g/cm^3 for 22 °C. Table 18 lists the homogenous Hamaker constants for the linoleum, polypropylene, and sodium fluorescein. The assumed value of the Hamaker constant for linoleum was based on the fact that typical values of the Hamaker constant for condensed phases (solid or liquid), interacting across vacuum, are $\approx10^{-19}$ J. When hydrocarbons are treated as an assembly of CH_2 groups, the value obtained for it is around 5×10^{-20} J (Martins et al. 2006). The Hamaker constant for sodium fluorescein was also assumed to be 5×10^{-20} J, since the molecules are composed of mostly C, H, and some O.

Table 18. The homogenous Hamaker constants of the floor materials and the particle used for calculating A_{132} for the chamber experiments.

Material	*A* (J)	Reference
linoleum-linoleum-air	5×10^{-20}	Assumed
polypropylene-polypropylene-air	7.1×10^{-20}	Martins et al. (2006)
Sodium fluorescein-sodium fluorescein-air	7.8×10^{-20}	Assumed

4.3.2 CFD Simulations of Particle Transport and Resuspension

After the flow field was calculated, particles were introduced into the domain from the bottom floor as a function of the friction velocity. The particle concentration was calculated assuming that particles were convected along with the flow, and the particle diffusivities were calculated using the Stokes-Einstein equation. Table 19 lists properties of particles as a function of the particle size. The diffusion coefficient is small for particles larger than 0.5 μm as compared to nano-sized particles. Gravitational settling could be significant for large-sized particles as seen from the gravitation terminal velocity. However, the effect of gravity was neglected in the simulations during Phase I, because scalar transport formulation cannot accommodate the effect of body forces, such as gravity, in the computational calculations. One can employ Lagrangian particle tracking ("spray" module) approach or Eulerian-Eulerian two-fluid ("two-fluid" module) model to include all the relevant forces affecting particle transport. Both of these capabilities are available in CFD-ACE+ and will be employed in Phase II work.

Table 19. Properties of particles as a function of the particle size.

Particle Size (μm)	Diffusivity (m^2/s)	Slip Correction Cc	Terminal Velocity (cm/s)	Relaxation Time (s)
0.01	5.39×10^{-8}	22.225	9.08×10^{-8}	9.26×10^{-9}
0.1	6.95×10^{-10}	2.867	1.17×10^{-4}	1.19×10^{-7}
0.5	6.45×10^{-11}	1.330	1.36×10^{-3}	1.39×10^{-6}
2.12	1.23×10^{-11}	1.077	1.98×10^{-2}	2.02×10^{-5}
4.04	6.24×10^{-12}	1.041	6.94×10^{-2}	7.08×10^{-5}
10.3	2.39×10^{-12}	1.016	4.41×10^{-1}	4.49×10^{-4}

Particle transport subsequent to resuspension was calculated for the fan flow rates of 20 and 132 L/min. A source term for particle was calculated using EC I, assuming the particle size was 0.5 μm and the initial deposition mass of the particle was 352 ng (0.06 ng/cm^2). Linoleum was the floor material. The resuspension at time 0 was assumed zero and resuspension started at 1 second; Figure 16 shows the particle source from resuspension.

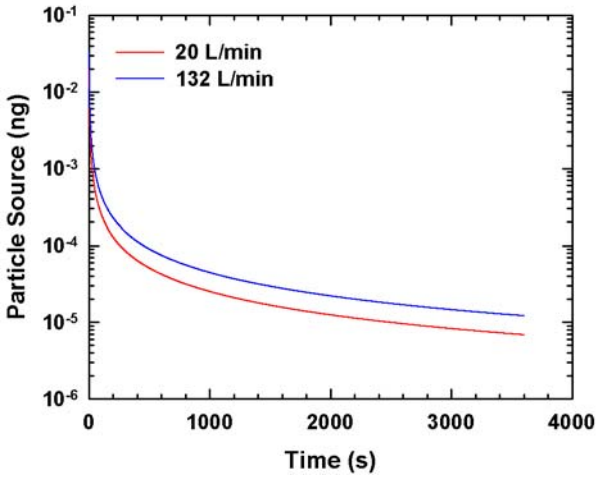

Figure 16. Particle source from the floor as a function of time. The particle source was calculated using the resuspension rate given by the empirical correlation, EC I. The particle size was 0.5 μm, and the initial deposition amount was 352 ng (0.06 ng/cm²). The floor material was linoleum.

For the same condition, Figure 17 shows the temporal and spatial evolutions of the particle concentration in the plane of the floor and in the plane along the diagonal of the chamber for 4 – 30 seconds; Figure 18 shows the same temporal and spatial evolutions for 60 – 240 seconds. Figure 19 shows temporal variations of particle concentration at the exit of bottom hole (for the APS). The particle concentration was predicted to reach a maximum in a very short time scale (~< 60s) and then to slowly decrease as the source term became smaller (as the resuspension rate decreased over time) and particle loss through the flow outlets continued.

4.4 Comparisons of Resuspension Data between Simulations and Measurement

Section 4.3.2 (p 48) presented the CFD simulation results of the particle concentration for 0.5 μm-sized particles over time. The simulations demonstrated that the empirical correlation of the particle resuspension rate could be coupled with CFD based code as a source term and the temporal and spatial evolution of the particle concentration could be obtained using CFD. In reality, all particles, whether biological warfare agents (BWA) or common dust particles, have size distributions. In the experiments on which the CFD simulations were based, the APS measured the particle concentration in 51 different size bins in the range of 0.5 – 20 μm and sodium fluorescein powder showed a size distribution between 0.5 and 15 μm.

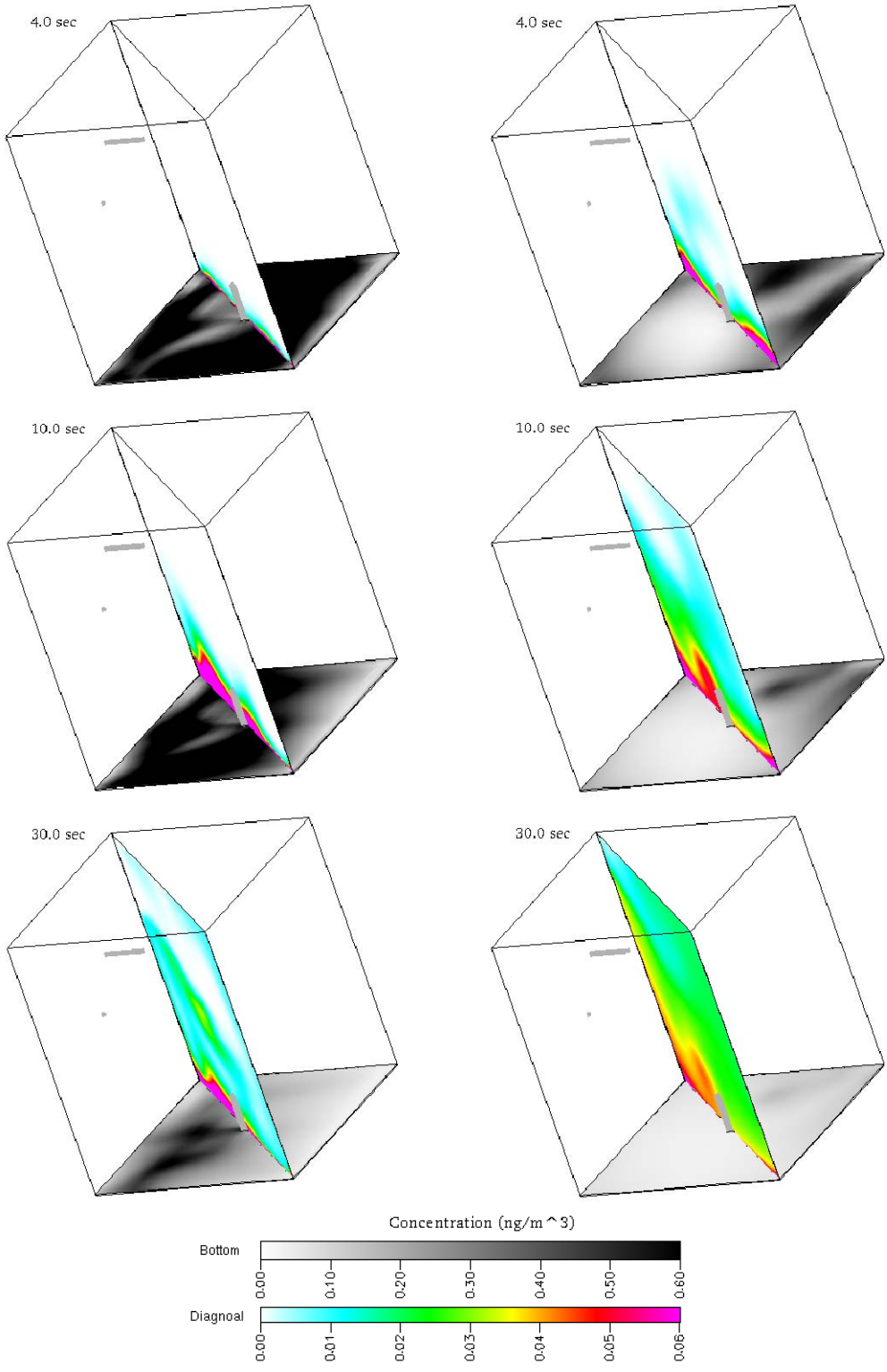

Figure 17. Isocontours of particle concentration in a plane at the floor and in a plane along the diagonal of the chamber showing spatial and temporal evolution of particle concentration between 4 and 30 seconds: at 20 L/min (left) and 132 L/min (right). The particle size was 0.5 μm, and the initial deposition amount was 352 ng (0.06 ng/cm²). The floor material was linoleum.

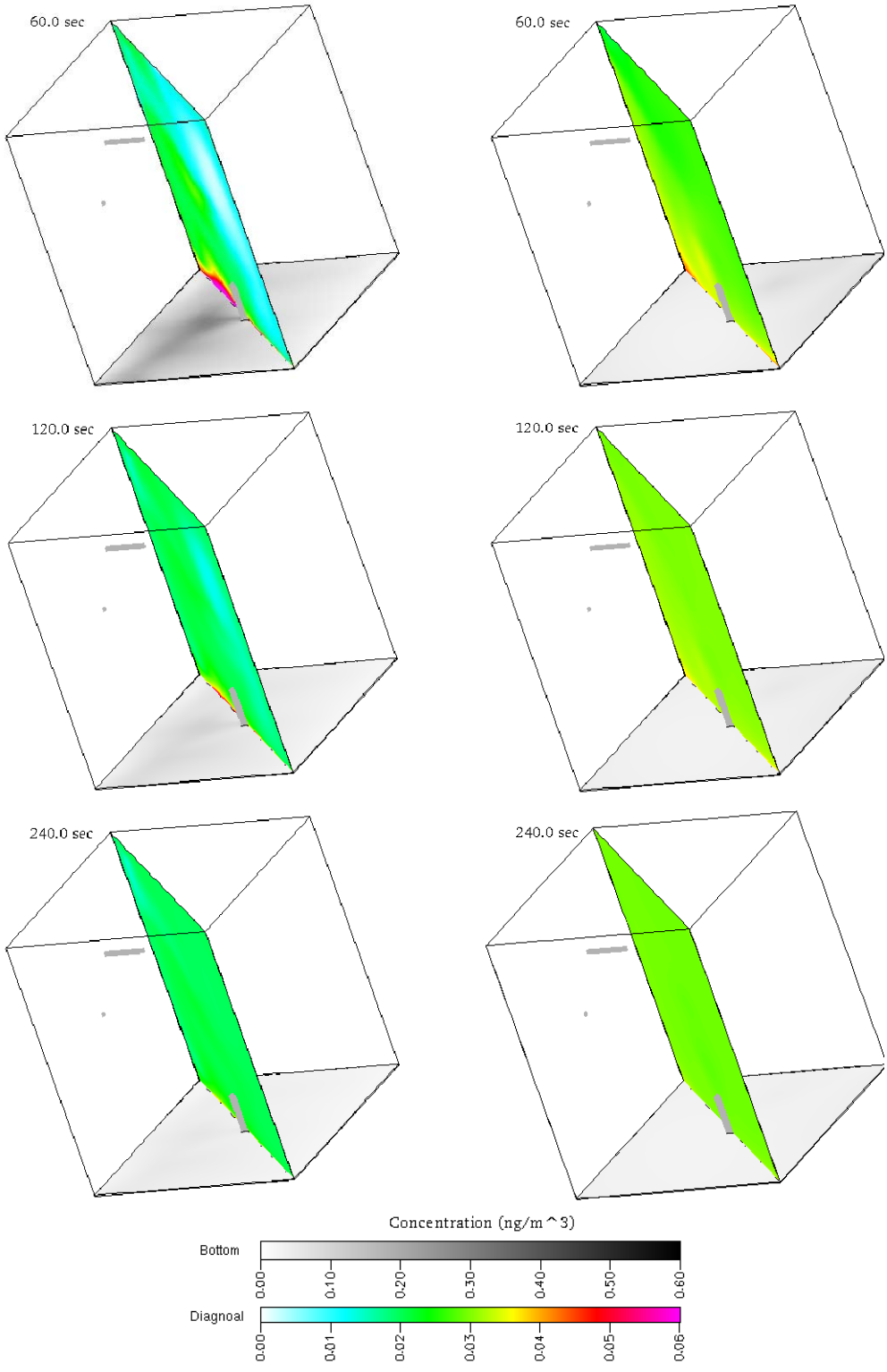

Figure 18. Isocontours of particle concentration in a plane at the floor and in a plane along the diagonal of the chamber showing spatial and temporal evolution of particle concentration between 60 and 240 seconds: at 20 L/min (left) and 132 L/min (right); the particle size was 0.5 μm, and the initial deposition amount was 352 ng (0.06 ng/cm²); the floor material was linoleum.

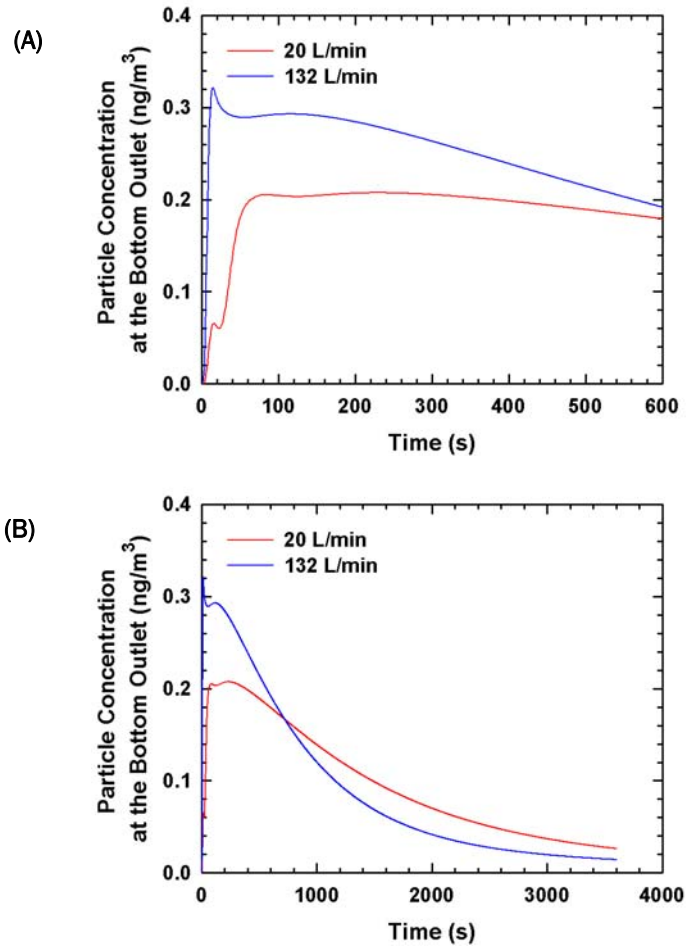

Figure 19. Time evolution of the particle concentration at the outlet located 5.25 in. above the floor at the center between (A) 0 – 600 s and (B) 0 – 3600 s; the particle size was 0.5 μm, and the initial deposition amount was 352 ng (0.06 ng/cm2); the floor material was linoleum.

Therefore, to compare with the experimental results, the CFD simulations in Section 4.3.2 (p 48) needed to be carried out for ~ 50 different particle sizes. Although it is certainly possible, it would take massive computational power and long computing time beyond the scope of the Phase I work. However, a simpler calculation can be done to compare with the experimental results, if it does not account for redeposition due to gravitational settling.

From Equation 77, the mass flux of particles at a given size is:

$$\text{Mass Flux}(d_p) = 8.521\times10^{-3}\frac{u_*^{0.5787} d_p^{1.2311} \rho_a^{0.5989}}{t^{1.0135}\rho_p^{0.3028} z_0^{0.3269} A_{132}^{0.2961}} \times \text{Inital Mass Depostion Density}(d_p) \quad \text{Eq 79}$$

Then, the mass resuspended during 1 hr for a given particle size is:

$$\text{Mass Resuspended} = 8.521\times10^{-3}\frac{d_{\text{p}}^{\,1.2311}\rho_{\text{a}}^{\,0.5989}}{\rho_{\text{p}}^{\,0.3028}z_0^{\,0.3269}A_{132}^{\,0.2961}}\times\sum_{\text{Mesh Area}}u_*^{\,0.5787}\times(\text{Mesh Area for }u_*)$$

$$\times\,\text{Inital Mass Deposition Density}\times\int_1^{3600}t^{-1.0135}dt \qquad \text{Eq 80}$$

Because the exponent of t is >1, 1 is used instead of 0 as the lower limit of the integration to avoid division by 0. It is the same reason that the resuspension at time 0 was assumed to equal zero and the resuspension started at 1 second in the CFD simulations.

The experiments were conducted for the resuspension of particles in the size range 1.7 – 3.8 μm and 5.0 – 10.3 μm, separately, from the floor covered with either linoleum or carpet. However, the results reported the data from the small (1.7 – 3.8 μm) and the large particles (5.0 – 10.3 μm) combined. Figure 20 shows the initial mass deposition density for linoleum and carpet. The small peaks between 2 and 3 μm in both cases were the result of combining the initial mass deposition densities of the small and the large particles.

For comparison, Figures 21-23 show the prediction from EC I against the experimental data with various fan settings for two different floor materials. The fraction of mass resuspended was calculated for individual particle sizes (the ratio of the total mass resuspended during 1 hr to the mass of initial deposition on the floor for a given particle size). For the experimental results, the mass resuspended during 1 hr was a measured value. For the predictions using EC 1, the mass resuspended was calculated using Equation 80. In some predictions, the lower and upper limits of the integration used were different from those specified in Equation 80 for the reasons described below.

As mentioned earlier, each resuspension experiment lasted 5 hrs, 1 hr with the fans off and 1 hr for each of four fan speeds (45, 75, 110, and 140). Particle resuspension was not observed in any experiment when the fans were off or at speed 45. Figure 21 shows the experimental results and the predictions for the fan speed of 75. The measured fan flow rate was 20 L/min for the experiments. The red circles were the prediction using EC I with the friction velocity obtained from the CFD simulation at 20 L/min fan flow rate.

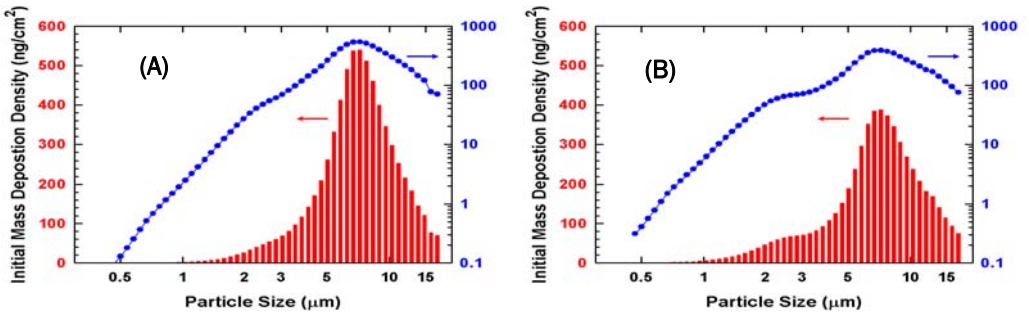

Figure 20. The initial mass deposition density as a function of particle size on (A) linoleum and (B) carpet.

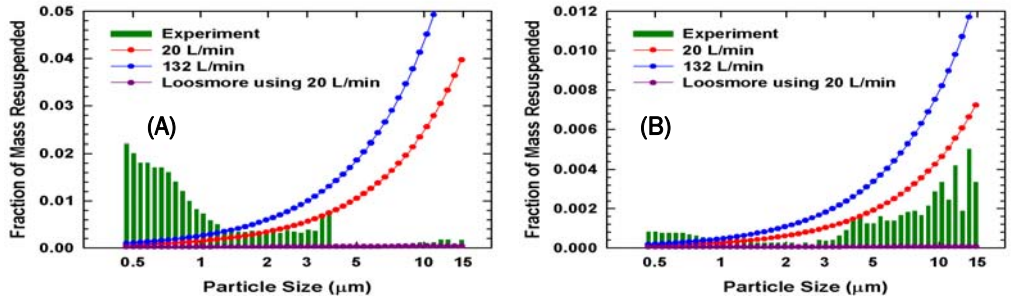

Figure 21. The total fraction of mass resuspended during 1 hr of resuspension experiment for (A) linoleum and (B) carpet. The fraction of mass resuspended was calculated for a given particle size as the ratio of the mass of particle resuspension to the mass of initial deposition on the floor. The fan setting was 75, and the measured fan flow rate was 20 L/min. The red and the blue circles indicate predictions using EC I at 20 L/min and 132 L/min, respectively, of the fan flow rate. The purple circles represent the prediction using the empirical correlation given by Loosmore (2003) using 20 L/min as the fan flow rate.

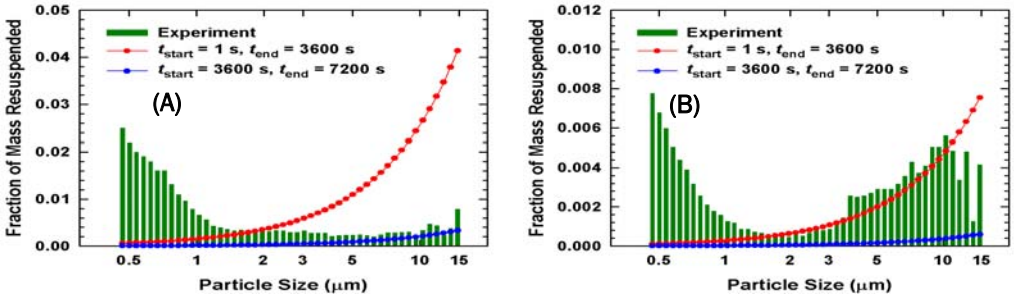

Figure 22. The total fraction of mass resuspended during 1 hr of resuspension experiment for (A) linoleum and (B) carpet. The fraction of mass resuspended was calculated for a given particle size as the ratio of the mass of particle resuspension to the mass of initial deposition on the floor. The fan setting was 110, and the measured fan flow rate was 40 L/min. The red and the blue circles indicate predictions using EC I at 40 L/min fan flow rate, and t_{start} and t_{end} specify the lower limit and the upper limit, respectively, of the integration in Eq 80.

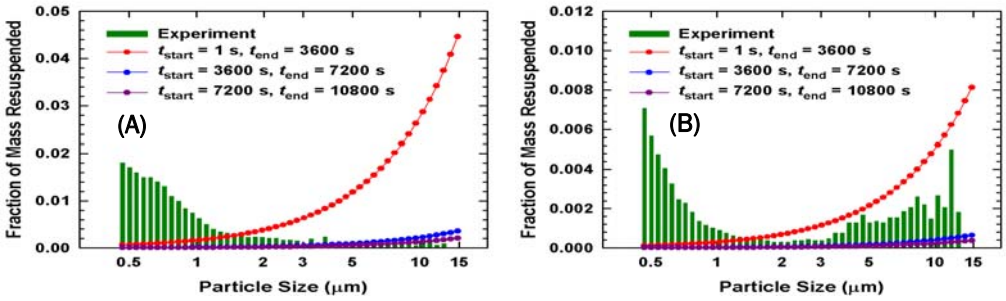

Figure 23. The total fraction of mass resuspended during 1 hr of resuspension experiment for (A) linoleum and (B) carpet. The fraction of mass resuspended was calculated for a given particle size as the ratio of the mass of particle resuspension to the mass of initial deposition on the floor. The fan setting was 140, and the measured fan flow rate was 70 L/min. The red, the blue, and the purple circles indicate predictions using EC I at 60 L/min of the fan flow rate, and t_{start} and t_{end} specify the lower limit and the upper limit, respectively, of the integration in Eq 80.

Since the particle resuspension did not occur before setting the fan speed at 75, researchers assumed that the time = 0 at the beginning of the experiments and used 1 and 3600 s as the lower and the upper limit of the integration in Equation 80. For linoleum floor, EC I (using 20 L/min) predicted reasonably well for particles between 2 and 4 μm. However, the experimental results for the particles larger than 4 μm were much lower than the prediction. Note that, for the experiments with linoleum floor, there was the discontinuity in that data between the small and the large particle experiments for the fan speed 75. This discontinuity is the reason for the abrupt decrease in the fraction of mass resuspended of the experiment for the particles larger than 4 μm in Figure 21(A); also the experimental results for the large particles were thought to be inaccurate. For the carpet, prediction by EC I (using 20 L/min) was slightly higher than the experiment for the particle larger than 2 μm (Figure 21[B]). For the particles smaller than 1 μm, the experimental results were higher than the predictions on both linoleum and carpet.

During the flow field simulation, the disagreement between the measured average velocity and the predicted velocity by CFD simulations in the plane 10 cm above the floor for a specified fan flow rate were noted. At 20 L/min fan flow rate, the average velocity from the CFD simulation was lower than the measured values. Therefore, the friction velocity obtained from the CFD simulation using 20 L/min would be lower than the friction velocity inferred from the measured average velocity. In Section 4.3.2 (p 48), the fan flow rate was increased up to 132 L/min in an effort to match the measured average velocity at 20 L/min. However, at 20 L/min,

the average velocity predicted from the CFD simulation using 132 L/min was still lower than the measured average velocity from the experiment.

Nevertheless, the friction velocity from the simulation with 132 L/min was used to predict particle resuspension. The purpose was to examine the effect if the fan flow rate measurement was erroneous and the average velocity measurement was accurate in the experiments. Because the friction velocities at 132 L/min is higher than that at 20 L/min, as one can expect, the fraction resuspended predicted using 132 L/min fan flow rate was higher than that predicted using 20 L/min (Figure 21). Since the predicted values from 132 L/min were much higher than those from the experiments, it was decided that all the predictions would be calculated using the friction velocities from CFD simulations with the fan flow rate that was the same as the measured fan flow rate, not with the fan flow rate that agreed with the measured average velocity.

The fraction of mass resuspended was calculated using Loosmore's empirical correlation. Figure 21 shows the results. The predictions from EC I and Loosmore's empirical correlation were similar for the 0.5 μm-sized particles. However, for the 15 μm-sized particles, Loosmore's empirical correlation predicted the fraction resuspended two orders of magnitude lower than EC I.

Figure 22 shows the experimental results and the predictions from EC I at the fan speed of 110. The measured fan flow rate was 40 L/min, and the predictions used the friction velocities from CFD simulations with 40 L/min. Because the experiments at the fan speed of 110 were conducted right after the experiments at 75 fan speed for an hour, it was not clear how to set the time span for these experiments. If one assumes the previous experiment at the fan speed of 75 did not have any influence on the experiment at the fan speed of 110, the time span for the experiment should be 0 – 1 hr. If the previous experiment had affected the experiment at the fan speed of 110, it would have resulted in lowering the fraction resuspended (at the fan speed of 110) compared to an experiment at the fan speed of 110 that is conducted independently. In that case, it may be more realistic to use the time span of 1 – 2 hr to predict the experiment at 110. For the linoleum floor, using the time span of 1 – 2 hr agreed better with the experimental results than using the time span of 0 – 1 hr for large particles (>5 μm). In contrast, the time span of 0 – 1 hr provided comparable results to the experiments on the carpet for the particles larger than 2 μm.

For the particles smaller than 1 μm, EC I underestimated the resuspended fraction regardless of floor materials and time span used.

Figure 23 shows the experimental results and the predictions from EC I at the fan speed of 140. The measured fan flow rate was 70 L/min, and the predictions used the friction velocities from CFD simulations with 60 L/min. The experiments with the fan speed of 140 followed the experiments with the fan speed of 110 so assigning the time span for the experiments was also a concern. Three different time spans (0 – 1 hr, 1 – 2 hr, and 2 – 3 hr) were used for the empirical correlations. For the linoleum floor, again, the result of 1 – 2 hr or 2 – 3 hr agreed better with the experimental results than the result of 0 – 1 hr for large particles. On the carpet, the time span of 0 – 1 hr gave a closer result to the experiment than 1 – 2 or 2 – 3 hr.

In conclusion, EC I predicted the experiments reasonably well for particles larger than 3 – 5 μm and underestimated the resuspension fraction for particles smaller than 1 μm in all conditions. Because the experiments were carried out sequentially with increasing fan speed, designating the time span of integration in Equation 80 for the subsequent experiments was an issue. For the linoleum floor, time counting from the first experiment gave better agreement with the experiments. This indicated that the previous experiment may have influenced the results of the following experiments. For the carpet, time counting from the first experiment did not agree well with the experiments. Instead, the time span of 0 – 1 hr worked acceptably for the subsequent experiments. For future experiments, different fan speed experiments should be carried out independently to remove any ambiguity in assign the time for resuspension.

Note that the friction velocities used for predicting the resuspension fraction were from the CFD simulations assuming a smooth surface without accounting for the surface roughness. If the surface roughness were included in the CFD simulations for the flow field calculation, the friction velocities would have been different. Consequently, it would have resulted in different predictions of the resuspended fraction. The prediction did not include the particle redeposition due to gravitational settling, which may have overestimated the resuspension fraction. It is anticipated that these issues will be addressed during Phase II of this project.

5 Summary, Conclusions, and Recommendations

5.1 Summary

In Phase I, Triton Systems developed empirical correlations that can predict the particle resuspension rate as a function of time, the friction velocity, the particle size, the particle density, the surface roughness, and the Hamaker constant, which represents van der Waals interaction between the particle and the surface. These parameters were selected based on the relevant mechanisms for resuspension phenomena, and the empirical correlations were expressed in dimensionless numbers. A physics-based model using the moment balance between adhesion and removal forces was also developed. The empirical correlations were tested against experimental data available in literature. Finally, the CFD simulations of the flow field were performed in a chamber where particle resuspension experiments were conducted. The CFD simulations of the particle resuspension and transport in the chamber were also carried out for one particle size with different floor materials. The resuspended fractions predicted by the empirical correlation EC I using the friction velocities from the flow field simulations was compared to the experimental results, and the prediction agreed reasonably well with the experiments.

5.2 Conclusions

Among the seven empirical correlations derived in Phase I, three correlations (EC I, EC IV, and EC VII) were physically realistic. EC I and EC IV expressed the resuspension rate as a function of time, the friction velocity, the diameter and the density of particles, the surface roughness, the Hamaker constant, and the density of air. The difference between EC I and EC IV was the method used to assign the reference time for the resuspension rate that was calculated from the fraction removal over time. EC I used the mid-point time as the representative time, and EC IV used the time t' that divided the area under the $1/t$ curve for a given time interval into two equal areas. The resuspension rate in EC VII was a function of time, friction velocity, diameter and density of particles, surface roughness, and the density and viscosity of air. EC VII employed the same approach to obtain the representative time for the resuspension rate as EC IV. These three empirical correlations predicted experimental data from the literature reasonably well. For some sets of data, the ratio of the pre-

dicted to the observed resuspension rates was centered at 1 and scattered within the range of one order of magnitude in either direction. However, the correlations underestimated the resuspension rate for other sets. The predictions from the three empirical correlations were comparable, and their performances were acceptable overall.

The models that used t' as the representative time were expected to yield better correlations than those that used the mid-point time. In fact, using t' did not show any advantageous results over using the mid-point. Although EC I, EC IV, and EC VII are equally valid to predict the resuspension rate, researchers slightly preferred EC I due to the fact that it uses the simple mid-point for the representative time and includes the Hamaker constant, which accounts for the material interactions between a surface and particles. One disadvantage of EC I is that the Hamaker constants for some materials are not readily available.

5.3 Recommendations

The quality of an empirical correlation depends on the data used to draw the correlations. Therefore, to model and predict the indoor resuspension accurately it would be essential to derive models based on the experimental data with the conditions that are characteristic to indoor resuspension. The empirical correlations developed in Phase I can be refined with better experimental data.

The physics-based model suggests the group of dimensionless numbers that were slightly different than those obtained for the empirical correlations. It is worthwhile to derive another empirical correlation based on the dimensionless numbers from the physics-based model and compare the performance with the empirical correlations obtained in Phase I.

References

Anspaugh, L. R., J. H. Shinn, P. F. Phelps, and N. C. Kennedy. (1975). "Resuspension and Redistribution of Plutonium in Soils." *Heath Physics*, vol 29, pp 571-582.

Anspaugh, L. R., S. L. Simon, K. I. Gordeev, I. A. Likhtarev, R. M. Maxwell, and S. M. Shinkarev. (2002). "Movement of Radionuclides in Terrestrial Ecosystems by Physical Processes." *Heath Physics*, vol 82, pp 669-679.

Biasi, L., A. de los Reyes, M. W. Reeks, and G. T. de Santi. (2001). "Use of a Simple Model for the Interpretation of Experimental Data on Particle Resuspension in Turbulent Flows," *Aerosol Science*, vol 32, pp 1175-1200.

Braaten, D. A. (1994). "Wind Tunnel Experiments of Large Particle Reentrainment-Deposition and Development of Large Particle Scaling Parameters." *Aerosol Science Technology*, vol 21, pp 157-169.

Braaten, D. A., U. K. T. Paw, and R. H. Shaw. (1990). "Particle Resuspension in a Turbulent Boundary Layer—Observed and Modeled." *Journal of Aerosol Science*, vol 21, pp 613-628.

Clever, J. W., and B. Yates. (1973). "Mechanism of Detachment of Colloidal Particles from a Flat Substrate in a Turbulent Flow." *Journal of Colloid and Interface Science*, vol 44, pp 464-474.

Corn, M., and F. Stein. (1965). "Re-Entrainment of Particles from a Plane Surface." *Journal of the Air Pollution Control Association*, vol 11, pp 566-575.

Davies, C. N. (1966). *Aerosol Science*. Academic Press, London, UK, p 384.

Davies, J. T. (1972). *Turbulence Phenomena*. Academic Press, New York, NY.

French, R. H. (2000). "Origins and Applications of London Dispersion Forces and Hamaker Constants in Ceramics." *Journal of the American Ceramic Society*, vol 83, pp 2117-2146.

Gadgil, A. J., E. U. Finlayson, M. L. Fisher, P. N. Price, T. L. Thatcher, M. J. Craig, K. H. Hong, J. Housman, C. A. Schwalbe, D. Wilson, J. E. Wood, and R. G. Sextro. (June 2000). *Pollutant Transport and Dispersion in Large Indoor Spaces: A Status Report for the Large Space Effort of the Interiors Project*. LBNL-44791.

Garland, J. A. (1979). *Resuspension of Particulate Matter from Grass and Soil*. UK Atomic Energy Authority, AERE_R 9452, HMSO. London.

Giess, P., A. J. H. Goddard, and G. Shaw. (1997). "Factors Affecting Particle Resuspension from Grass Swards." *Journal of Aerosol Science*, vol 28, pp 1331-1349.

Gomes, C., J. Freihaut, and W. Bahnfleth. (2005). *Resuspension of Allergen-Containing Particles under Mechanical and Aerodynamic Disturbances from Human Walking: Introduction to an Experimental Controlled Methodology*. Indoor Environment Center, Architectural Engineering Department, Pennsylvania State University, accessible through URL: http://www.engr.psu.edu/ae/iec/publications/papers/resuspension_of_allergen_containing_particles.pdf

Hall, D. (1988). "Measurements of the Mean Force on a Particle near a Boundary in Turbulent Flow." *Journal of Fluid Mechanics*, vol 187, pp 451-466.

Hallas, Kevin, and Robert Shaw. (2006). *Evaluation of the Kirchberg Rolling Slider and SlipAlert Slip Resistance Meters*. HSL/2006/65, Health and Safety Laboratory, Harpur Hill, Buxton, Derbyshire, UK, accessible through URL: www.hse.gov.uk/research/hsl_pdf/2006/hsl0665.pdf

Hinds, W. C. (1999). *Aerosol Technology: Properties, Behavior, and Measurement of Airborne Particles*. 2d ed. John Wiley & Sons, Inc. New York, NY.

Hu, B., J. D. Freihaut, W. Bahnfleth, C. A. S. Gomes, and B. Thran. (2005). "Literature Review and Parametric Study: Indoor Particle Resuspension by Human Activity." *Proceedings of the 10th International Conference on Indoor Air Quality and Climate, Beijing, China*.

Ibrahim, A. H. (2004). *Microparticle Detachment from Surfaces by Fluid Flow*. Ph.D. thesis, Notre Dame, in.

Johnson, K. L., K. Kendall, and A. D. Roberts. (1971). "Surface Energy and the Contact of Elastic Solids." *Proceedings of the Royal Society A*, vol 324, pp 301-313.

Jurcik, B., and H-C. Wang. (1991). "The Modelling of Particle Resuspension in Turbulent Flow." *Journal of Aerosol Science*, vol 22, pp S149-S152.

Krauter P., and A. Biermann. (2007). "Reaerosolization of Fluidized Spores in Ventilation Systems." *Applied and Environmental Microbiology*, vol 73, pp 2165-2172.

Leighton, D. T, and A. Acrivos. (January 1985). "The Lift on a Small Sphere Touching a Plane in the Presence of a Simple Shear Flow." *Journal of Applied Mathematics and Physics (ZAMP)*, vol 36, pp 174-178.

Lengweiler, P. (2000). *Modelling Deposition and Resuspension of Particles on and from Surfaces*. Ph.D. thesis. Swiss Federal Institute of Technology, Zürich, Switzerland.

Lengweiler, P., P. Nielsen, A. Moser, P. Heiselberg, and H. Takai. (1998). "Deposition and Resuspension of Particles: Which Parameters Are Important?" *Roomvent '98 Conference, Stockholm*, vol 1, pp 317-323.

Linsley, G. S. (1978). *Resuspension of the Transuranium Elements—A Review of Existing Data*. NRPB -75, HMSO, National Radiological Protection Board (NRPB), London, UK.

Loosmore, G. A. (2003). "Evaluation and Development of Models for Resuspension of Aerosols at Short Times after Deposition." *Atmospheric Environment*, vol 37, pp 639-647.

Martins, J. A., W. Zhang, and A. M. Brito. (2006). "Saturation of Shear-Induced Isothermal Crystallization of Polymers at the Steady State and the Entanglement-Disentanglement Transition." *Macromolecules*, vol 39, No. 22, pp 7626-7634.

National Council on Radiation Protection & Measurements (NCRP). (1999). *Recommended Screening Limits for Contaminated Surface Soil and Review of Factors Relevant to Site-Specific Studies*. NCRP Report No. 192.

Nicholson, K. W. (1988). "A Review of Particle Resuspension." *Atmospheric Environment*, vol 22, pp 2639-2651.

Nicholson, K. W. (1993). "Wind Tunnel Experiments on the Resuspension of Particulate Material." *Atmospheric Environment*, vol 27A, pp 181-188.

Punjrath, J. S., and D. R. Heldman. (1972). "Mechanisms of Small Particle Re-Entrainment from Flat Surfaces." *Aerosol Science*, vol 3, pp 429-440.

Reeks, M. W., and D. Hall. (2001). "Kinetic Models for Particle Resuspension in Turbulent Flow: Theory and Measurement." *Journal of Aerosol Science*, vol 32, pp 1-31.

Reeks, M. W., J. Reed, and D. Hall. (1988). "On the Resuspension of Small Particles by a Turbulent Flow." *Journal of Physics D: Applied Physics*, vol 21, pp 574-589.

Rijnaarts, H. H. M., W. Norde, E. J. Bouwer, J. L. Lyklema, and A. J. B. Zehnder. (1995). "Reversibility and Mechanism of Bacterial Adhesion." *Colloids Surf B Biointerfaces*, vol 4, pp 5–22.

Saffman, P. G. (1965). "The Lift Force on a Small Sphere in A Slow Shear Flow." *Journal of Fluid Mechanics*, vol 22, pp 385-400.

Saffman, P. G. (1968). "Corrigendum." *Journal of Fluid Mechanics*, vol 31, p 624.

Sehmel, G. A. (1980). "Particle Resuspension: a Review." *Environment International*, vol 4, pp 107-127.

Sohn, C. W., A. Solberg, and T. Gonsoulin. (November 2004). *Analysis of Numerical Models for Dispersion of Chemical/Biological Agents in Complex Building Environments*. ERDC/CERL TR-04-25, Engineer Research and Development Center, Construction Engineering Research Laboratory (ERDC-CERL), Champaign, IL.

Soltani, M., and G. Ahmadi. (2004). "On Particle Adhesion and Removal Mechanisms in Turbulent Flows." *Journal of Adhesion Science and Technology*, vol 8, pp 763-78.

Sutton, O. G. (1955). *Atmospheric Turbulence*. John Wiley, New York, NY, p 95.

Thatcher, T. L., and D. W. Layton. (1995). "Deposition, Resuspension, and Penetration of Particles with a Residence." *Atmospheric Environment*, vol 29, pp 1487-1497.

U.S. Army Environmental Command (USAEC). (1974). *Proposed Final Environment Statement, Liquid Metal Fast Breeder Reactor Programme*, Part II.G-19, WASH-1535, USAEC, Washington, DC.

USAEC. (1975). *Reactor Safety Study—An Assessment of Accident Risks in US Commercial Nuclear Power Plants.* Appendix IV. E-13, WASH-1400, USAEC, Washington, DC.

Wen, H. Y., and G. Kasper. (1989). "On the Kinetics of Particle Reentrainment from Surfaces." *Journal of Aerosol Science*, vol 20, pp 483-498.

Wu, Y-L., C. I. Davidson, and A. G. Russell. (1992). "Controlled Wind Tunnel Experiments for Particle Bounceoff and Resuspension." *Aerosol Science Technology*, vol 17, pp 245-262.

Zimon, A. D. (1969). "The Adhesion of Dust and Powder." *The Adhesion of Dust and Powder* (M. Corn, ed.), Plenum Press, New York, NY, pp 172-173.

Ziskind, G. (2006). "Particle Resuspension from Surfaces: Revisited and Re-Evaluated." *Reviews in Chemical Engineering*, vol 22, pp 1-123.

Ziskind, G., M. Fichman, and C. Gutfinger. (1995). "Resuspension of Particulates from Surfaces to Turbulent Flows—Review and Analysis." *Journal of Aerosol Science*, vol 26, pp 613-644.

Acronyms, Abbreviations, and Terms

Term	Spellout
AFM	atomic force microscopy
APS	Aerodynamic Particle Sizer
BWA	biological warfare agents
CB	chemical and biological
CERL	Construction Engineering Research Laboratory
CFD	computational fluid dynamics
CFDRC	CFD Research Corporation
DC	direct current
EC	Engineer Circular
EC	Empirical correlation
ERDC	Engineer Research and Development Center
ESI	Environmental Sustainability Index
FC	Facility Composer
FD	Forced Draft
FY	fiscal year
HVAC	heating, ventilating, and air-conditioning (HVAC)
IAQ	indoor air quality
JKR	Johnson-Kandall-Roberts (model)
LBNL	Lawrence Berkeley National Laboratory
MIPR	Military Interdepartmental Purchase Request
NCRP	National Council on Radiation Protection & Measurements
NRPB	National Radiological Protection Board
PVC	polyvinyl chloride
RH	relative humidity
RH	Relative humidity
SBIR	Small Business Innovative Research
SS	Stainless Steel
TNT	trinitrotoluene
TR	Technical Report
UK	United Kingdom
URL	Universal Resource Locator
USAEC	U.S. Army Environmental Command
WWW	World Wide Web

A_{132}	Hamaker constant for Particle 1 and Surface 2 in Medium 3
a	Rate constant
*a*0	Coefficient in empirical correlation

Term	Spellout
$a1$	Coefficient in empirical correlation
$a2$	Coefficient in empirical correlation
$b0$	Coefficient in empirical correlation in EC I and EC IV
$b1$	Coefficient in empirical correlation in EC I and EC IV
$b2$	Coefficient in empirical correlation in EC I and EC IV
$b3$	Coefficient in empirical correlation in EC I and EC IV
$b4$	Coefficient in empirical correlation in EC I and EC IV
$c0$	coefficient in empirical correlation in EC II and EC V
$c1$	Coefficient in empirical correlation in EC II and EC V
$c2$	Coefficient in empirical correlation in EC II and EC V
$c3$	Coefficient in empirical correlation in EC II and EC V
C_{fx}	Local shear stress coefficient
$d0$	Coefficient in empirical correlation in EC III, EC VI, and EC VII
$d1$	Coefficient in empirical correlation in EC III, EC VI, and EC VII
$d2$	Coefficient in empirical correlation in EC III, EC VI, and EC VII
$d3$	Coefficient in empirical correlation in EC III, EC VI, and EC VII
$d4$	Coefficient in empirical correlation in EC III, EC VI, and EC VII
$d5$	Coefficient in empirical correlation in EC III, EC VI, and EC VII
d_h	Hydraulic diameter
d_p	Particle diameter
E_1	Young's modulus for particle
E_2	Young's modulus for surface
F	Ratio of adhesion force to removal force
F_{adh}	Adhesion force
F_C	Capillary force
F_D	Drag force
F_{EDL}	Electrostatic force due to electrostatic double layer
F_L	Lift force
F_Q	Electrostatic force due to a charged particle
F_{vdW}	van der Waals force
g	Gravity
K	Resuspension factor
k	Turbulent kinetic energy
M	Ratio of adhesion moment to removal moment
N	Particle number density on surface
N_0	Number density of particles on surface at time 0
N_T	Total particle number density on surface
p_t	Turbulent pressure
q	Charge on particle
r_a	Contact radius
r_{a0}	Contact radius at zero applied load
$r_{adhesion}$	Adhesion radius

Term	Spellout
r_p	Particle radius
s	Separation distance between the particle and the surface
t	Time
U_∞	Free stream velocity
u_*	Friction velocity
V_d	Turbulent deposition velocity
z_0	Aerodynamic surface roughness length
ε	Turbulent intensity
ε_0	Dielectric constant
ϕ_c	Contact potential
$\dot{\gamma}$	Shear rate
γ_{LV}	Liquid-gas surface tension
φ	Diabatic influence function
κ	von Karman constant
Λ	Resuspension rate
μ_a	Viscosity of air
ν	Kinematic viscosity of air
ν_1	Poisson ratio of particle
ν_2	Poisson ratio of surface
ρ_a	Density of air
ρ_p	Particle density
σ	Surface energy
τ_w	Wall shear stress

REPORT DOCUMENTATION PAGE

Form Approved
OMB No. 0704-0188

1. REPORT DATE (DD-MM-YYYY)	2. REPORT TYPE	3. DATES COVERED (From - To)
17-02-2008	Final	

4. TITLE AND SUBTITLE
Source Term Model for Fine Particle Resuspension from Indoor Surfaces

5a. CONTRACT NUMBER

5b. GRANT NUMBER

5c. PROGRAM ELEMENT NUMBER

6. AUTHOR(S)
Yoojeong Kim, Ashok Gidwani, Mark Sippola, and Chang W. Sohn

5d. PROJECT NUMBER
SBIR

5e. TASK NUMBER

5f. WORK UNIT NUMBER

7. PERFORMING ORGANIZATION NAME(S) AND ADDRESS(ES)
U.S. Army Engineer Research and Development Center (ERDC)
Construction Engineering Research Laboratory (CERL)
PO Box 9005,
Champaign, IL 61826-9005

8. PERFORMING ORGANIZATION REPORT NUMBER
ERDC/CERL TR-08-4

9. SPONSORING / MONITORING AGENCY NAME(S) AND ADDRESS(ES)
U.S. Army Engineer Research and Development Center (ERDC)
Construction Engineering Research Laboratory (CERL)
PO Box 9005
Champaign, IL 61826-9005

10. SPONSOR/MONITOR'S ACRONYM(S)

11. SPONSOR/MONITOR'S REPORT NUMBER(S)

12. DISTRIBUTION / AVAILABILITY STATEMENT
Approved for public release; distribution is unlimited.

13. SUPPLEMENTARY NOTES

14. ABSTRACT

This Phase I effort developed a source term model for particle resuspension from indoor surfaces to be used as a source term boundary condition for CFD simulation of particle transport and dispersion in a building. Specifically, this work: (1) investigated responsible mechanisms for fine particle resuspension from indoor surfaces, (2) identified parameters relevant to resuspension, (3) performed a dimensional analysis and derivation of a resuspension model, and (4) evaluated the model against published experimental data on re-suspension. Preliminary validation of the derived model was conducted based on a set of experimental data from the Lawrence Berkeley National Laboratory.

15. SUBJECT TERMS
indoor air quality (IAQ) particle resuspension simulation modeling

16. SECURITY CLASSIFICATION OF:			17. LIMITATION OF ABSTRACT	18. NUMBER OF PAGES	19a. NAME OF RESPONSIBLE PERSON
a. REPORT	b. ABSTRACT	c. THIS PAGE			19b. TELEPHONE NUMBER (include area code)
Unclassified	Unclassified	Unclassified	SAR	80	